SLURRY EROSION OF ULTRA HIGH STRENGTH BAINITIC STEEL

A DISSERTATION

Submitted in partial fulfilment of the

requirements for the award of the degree

of

MASTER OF TECHNOLOGY

in

METALLURGICAL AND MATERIALS ENGINEERING
(With Specialization in Materials Engineering)

Submitted by

ANKIT YADAV

Department of Metallurgical and Materials Engineering

INDIAN INSTITUTE OF TECHNOLOGY, ROORKEE

ROORKEE – 247667 (INDIA)

MAY 2018

INDIAN INSTITUTE OF TECHNOLOGY

ROORKEE-247667

CANDIDATE'S DECLARATION

I hereby declare that the work which is being presented in the project entitled "SLURRY EROSION OF ULTRA HIGH STRENGTH BAINITIC STEEL" in partial fulfillment of the requirement for the award of the degree of Master of Technology in Materials Engineering, submitted in Department of Metallurgical and Materials Engineering, Indian Institute of Technology, Roorkee is an authentic record of my own work carried out for the period from July 2017 to May 2018 under the supervision of Dr. Sourav Das, Assistant Professor at the Department of Metallurgical and Materials Engineering, Indian Institute of Technology Roorkee.

The matter embodied in this report has not been submitted by me for the award of any other degree or diploma.

Dated:

Place: Roorkee **ANKIT YADAV**

CERTIFICATE

This is to certify that the above statement made by the candidate is correct to the best of my knowledge.

Dated: **Dr. SOURAV DAS**

Place: Roorkee Assistant Professor

MMED, IIT Roorkee

ACKNOWLEDGMENT

I wish to express my deep sense of gratitude and sincere thanks to my supervisor Dr. Sourav Das Metallurgical and Material Engineering Department, Indian Institute of Technology Roorkee, for their inspiration and active supervision and constant encouragement to complete my dissertation work. This work is simply the reflection of his thoughts, ideas, and concepts. Working under his guidance was a privilege and an excellent learning experience that I will cherish forever. I would like to thank Dr. S. K. Nath and Dr. K. S. Suresh for giving their valuable time to solve different problem during my project work. Also I wish to extend my sincere thanks to Mr. Suruj Protim Neog, Mr. Nilesh Paraye and Mr. Akeshwar, research scholors, IIT Roorkee for their excellent guidance and suggestions for the successful completion of my dissertation work. I also acknowledge the blessings of my parents and co-operation of my seniors, which is very valuable to me.

ABSTRACT

Newly developed ultra-high strength bainitic steels have very good mechanical properties and potential materials for heavy wear applications. In the current work, an effort has been made to determine erosion behaviour of ultra-high strength bainitic steel in slurry environment. The erosion wear tests were carried out on slurry pot erosion tester with different impact angles and time. 5 wt% slurry concentration is used for the test. The weight loss of the material measured after the erosion tests and worn surfaces were analysed by scanning electron microscopy. Surface roughness of the samples were also analysed before the tests so that initial condition remain same.

This dissertation includes six chapters in which **Chapter 1** gives the brief introduction of the ultra-high strength bainitic steel. **Chapter 2** gives the general description of the theoretical background of erosion. **Chapter 3** discusses about objective of present work. **Chapter 4** gives the description about the experimental methodology employed for this dissertation work. **Chapter 5** discusses about the results obtained for various experiments conducted. **Chapter 6** gives the conclusions of the overall dissertation work. Suggestions for future work and references are given at the end of the dissertation.

CONTENTS

LIST OF FIGURES

LIST OF TABLES

LIST OF ABBREVIATIONS

HSLA……..	High strength low alloy
Wt.%.....	Weight %
SEM…….	Scanning electron microscopy
EDX ……	Energy dispersive x-ray spectroscopy
XRF…….	X-ray fluorescence
et al……..	et alia
YS……	Yield strength
UTS…….	Ultimate tensile strength
Mpa…….	Mega pascal
VHN……	Vickers hardness number
AISI…….	American iron and steel institute
a.u…….....	Arbitrary unit
ASTM……..	American society for testing and materials

CHAPTER 1

INTRODUCTION

It is observed that the heavy damage in mineral processing, dredging, and transporting industries is caused due to erosion of steels by the impingement of solid particles in a fluid stream**.** Wear of pipelines and turbine blades made of carbon steel, manganese steel, and cast iron is very high due to low erosion resistance. [1–5] These materials easily get damage by high-speed stream of water with or without the impingement from solid particles. Different types of erosion tests are used to study the erosive wear behaviour of these materials. Current work is focused on analyzing the erosive behaviour of ultra-high strength bainitic steel developed by Das et al. [6] in the slurry environment. Composition and mechanical properties of the ultra-high strength bainitic steel is given in Table 1 and Table 2. Figure 1 shows the true and engineering stress-strain curve of the ultra-high bainitic steel.

Table 1: Composition of ultra-high strength bainitic steel [6]

Elements	C	Mn	Si	Cr	Al	Ti
wt. %	0.34	1.80	1.51	0.92	0.015	0.032

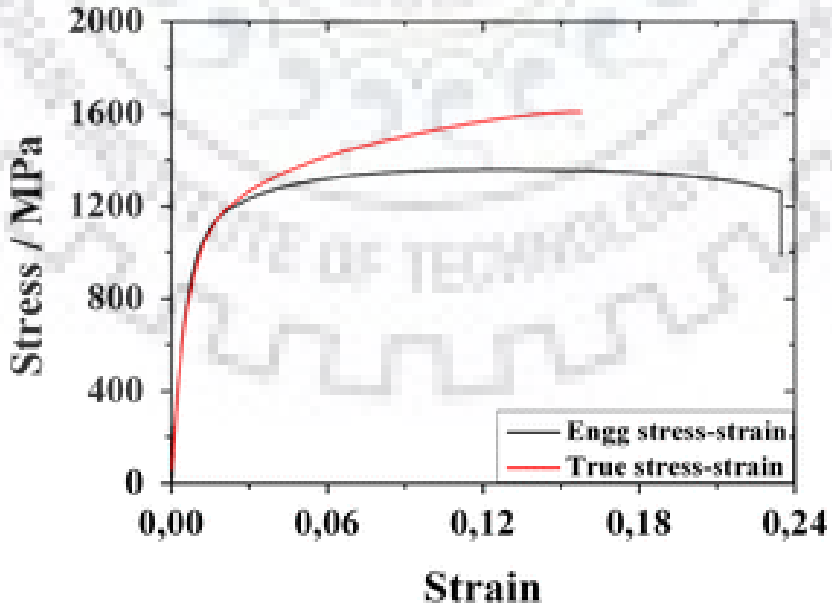

Fig 1: Stress- strain curve of ultra-high strength bainitic steel [6]

Table 2. Mechanical Properties of ultra-high strength bainitic steel.[6]

YS (MPa)	UTS (MPa)	Uniform Elongation (Percent)	Total Elongation (percent)	Hardness (VHN)
980±25	1385±15	13.6±0.5	22±1	413±9

We can see ultra- high strength bainitic steel has a good combination of strength and ductility but there is no wear data available, this work is focused on analyzing the erosion behaviour in the slurry environment.

CHAPTER 2

LITERATURE REVIEW

2.1 Wear

When surface of one material is eroded by another surface it is termed as wear in materials science. This type of surface interactions removes the material from the surface as a result of mechanical action. The basic difference in mechanical action and other processes with similar outcomes is that relative motion is required between the two surfaces. Wear can also be defined as a process in which interaction of the surfaces of material with its working environment results in dimensional loss of the solid, with or without loss of material. There are various aspects of the working environment which affect the wear. This include loads (such as unidirectional sliding, reciprocating, rolling, and impact loads), speed, temperature, type of counter body (solid, liquid, or gas), and type of contact (single phase or multiphase). [7]

2.1.1 Types of wear

There are four principal wear processes according to standard literatures [7]. These are mentioned and discussed below.

1. Abrasive wear
2. Adhesive wear
3. Erosive wear
4. Corrosive wear

2.1.1.1. Abrasive wear

Abrasive wear occurs due to sliding of a hard rough surface over a softer surface. ASTM defines it as the loss of material due to hard particles or hard protrusions that are pressed against and move along a solid surface Abrasive wear is generally classified according to the type of contact and the working environment.[8] The mode of abrasive wear can be determined by The type of contact. The two modes of abrasive wear are known as two-body and three-body abrasive wear as shown in Figure 2 (a) and 2(b). Two-body abrasive wear occurs when the grits, or hard abrasive particles, are rigidly mounted e to a surface remove the material from the counter surface. Three-body wear occurs when the hard abrasive articles or grits are not constrained and are free to

roll and slide down a surface.[7] The material is displaced or removed from the softer surface by combined action of micro ploughing & micro-cutting.

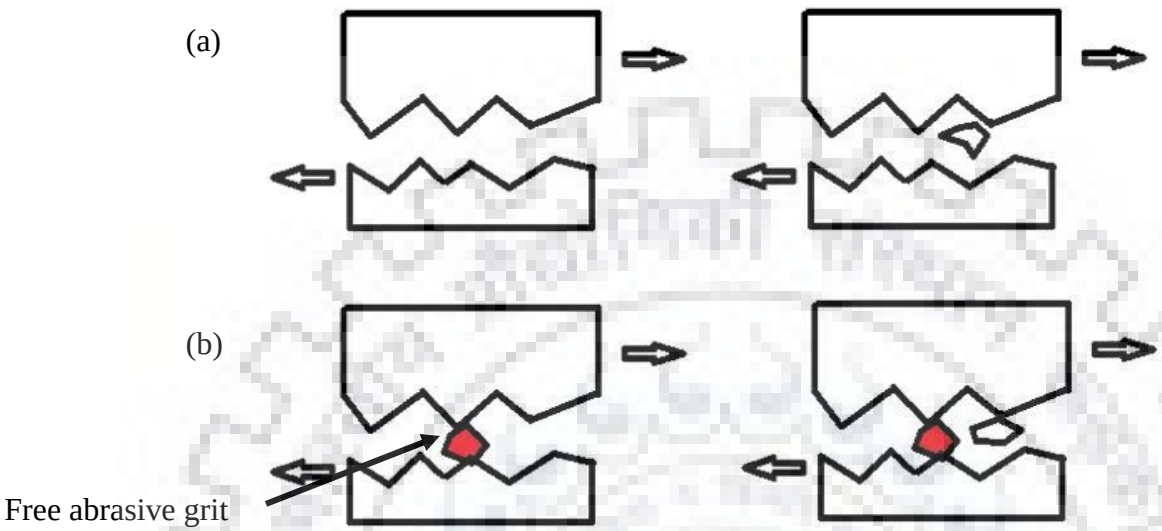

Fig 2: (a) Two body abrasive wear (b) Three body abrasive wear [7]

2.1.1.2 Adhesive wear

Adhesive wear is very common in metals and it is dependent on the mutual affinity between the materials. Adhesive wear occurs when two surfaces slide over each other, or are forced into one another. This causes material transfer between the two surfaces.[7] Adhesive wear can also be defined as plastic deformation occurred within the surface layer when two surfaces pushed against each other. Adhesive wear mechanism is shown in Figure 3.The asperities present in the mating surfaces will penetrate the opposing surface and develop micro-weld between them. Adhesive wear is a result or micro-weld formation between the opposing asperities caused by rubbing of surfaces of the counter bodies. These micro-joints forms due to very high load applied to the contacting asperities because of this they deform and adhere to each other. These micro-weld breaks due to relative motion between the contacting surfaces. The welded asperity also breaks in the non-deformed regions of the surface. Thus some of the material is get transferred by its counter body. This effect is known as scuffing or galling. [9]

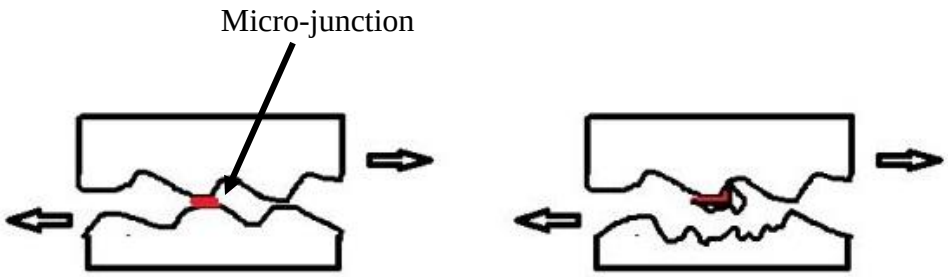

Fig 3: Adhesive wear [7]

2.1.1.3. Erosive wear

It is observed that erosion can occur by jets and streams of solid particles, liquid droplets, and implosion of bubbles formed in the fluid. Generally following types of erosion can be seen in practical situations:

- **Solid particle erosion**

Solid particle erosion occurs by impingement of solid particles at a velocity as shown in Fig 4. [7]

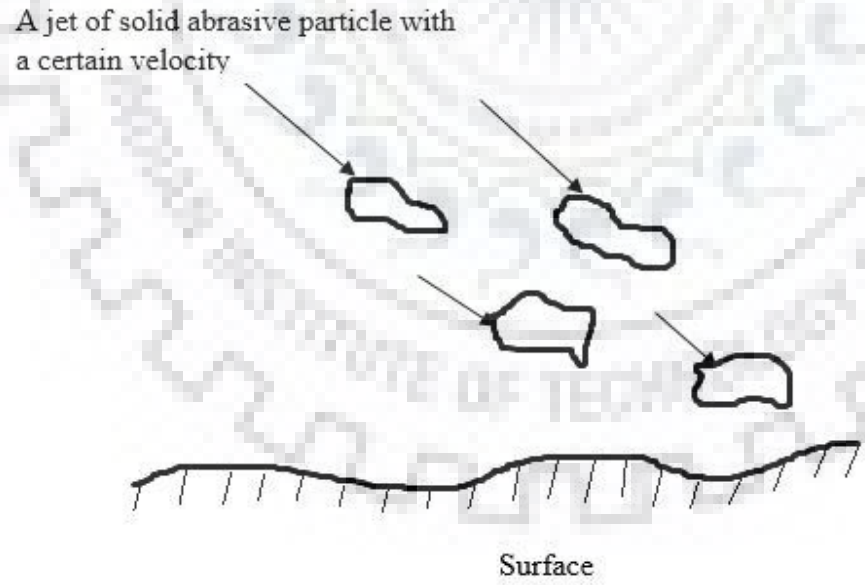

Fig 4: Schematic of a jet of erodent particles striking a surface at a high velocity.[7]

- **Liquid impingement erosion**

It is observed that liquid drops can also erode the surface if its strike with high velocity. If the striking velocity is very high than material will experience a very high pressure. This pressure can exceeds the yield strength of most materials causing heavy damage. [7]

- **Slurry erosion**

Slurry erosion is defined as the erosion wear of material caused by a stream of high velocity slurry consisting of solid abrasive particle in the liquid (usually water). Slurry erosion is discussed in detail in the next section.

- **Cavitation erosion**

Cavitation is defined as the formation of bubbles in a liquid. This is a repeated process of nucleation, growth, and violent collapse of cavities or bubbles in a liquid. It is observed that cavitation can occur in any liquid in which the pressure fluctuates. Cavitation erosion is the mechanical degradation of material caused by cavitation in liquid. When a liquid subjected to sufficiently high stress, vapour filled voids or cavities arc formed at weak regimes within the liquid. In practice all liquids contain gaseous and solid impurities, which act us nucleation sites for the cavities. When the liquid contain cavities is subsequently subjected to compressive stress that is to higher hydrostatic pressure these cavities will collapses, When a cavity collapses within, the body of the liquid, away from any solid boundary, it does so symmetrically and a emits a shock wave into surrounding liquid. On the other hand, those cavities that are either in contact with or close to the solid surface will collapse asymmetrically, forming a micro jet of liquid directed towards the solid. This collapse is directly responsible for the erosion process.[10]

2.1.1.4. Corrosive wear

It is observed that corrosive wear occurs when the working environment of the material has corrosive medium. Few studies shows that wear may be accelerated by the corrosion of the contacting surfaces. Chemical reactions occurs on the mating surfaces and product stays on the surface. These products get removed by the further rubbing and relative motion of the contacting surfaces. Hard oxide particles trapped between the mating surfaces can increase the wear rate by three body abrasive wear mechanism.[11]

2.1.2 Slurry erosion

A mixture of liquid and solid particles is generally known as slurry when it is ready for pumping related operations. From the above discussion we can see various types of erosion can be seen in high speed slurry transportation. In major industrial operations like dredging, pumping and large mining projects transporting minerals or solids as a slurry is an increasingly viable alternative. Slurry erosion wear causes material loss and huge amount of money spent every due to this type of erosion. Figure 5 shows the types of tester which can be used for slurry erosion study.

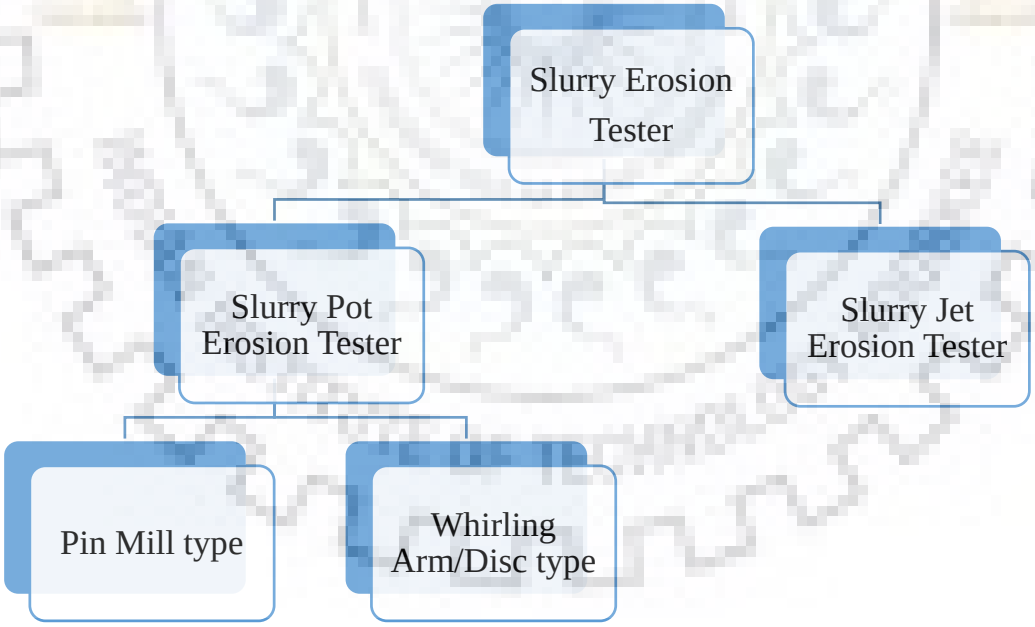

Fig 5: Types of slurry pot erosion tester

In the current work whirling disc type slurry pot erosion tester is used in which sample are kept in vertical position as compared to pin mill type in which sample is kept in horizontal position.

2.1.3 Parameters affecting slurry erosion:

- **Microstructure**

  Metallurgical hardness and microstructures are commonly interrelated and both have importance as factors in resistance to erosion. By increasing the carbon content of steel results in microstructural alteration that increases hardness and decreases ductility, impact strength and tensile toughness. The maximum hardness depends on the carbon Content of the steel and the amount or martensite, Carbon content also affects erosion resistance through formation of various carbides. Sometimes due consideration is not given to the development of adequate microstructure in the underwater components. Composition alone is not sufficient to impart proper erosion resistance in the steels.

- **Impingement angles**

  Few studies shows that impingement angles affect the slurry erosion differently for ductile and brittle materials. Yadav et al. [12] studies the slurry erosive wear of d-gun sprayed coatings on SAE 431 and concludes that Maximum erosion wear was occurred at 30° impact angle and minimum at 90°.

- **Time of exposure**

  Time of exposure is important parameter in slurry as few studies suggest that after some time ductile material tend to form work hardened layer which reduces the erosion rate also erodent particle get blunt with the passage of time. [13]

- **Rotational speed**

  Some researchers studies the slurry erosion by varying the rotational speed in the slurry pot tester. Singh et al. [13] studied the erosion wear in a slurry pipe with multisized coal and bottom-ash slurries on two materials namely mild steel and stainless steel 304 and concluded that the rotational speed was found to be most influence parameter in increasing the erosion wear rate.

- **Erodent particle size**

  It has been observed that when the particle size is increased, the mean free path of the abrasive particle decreases. This causes more particle–particle collisions before the

erodent particles reached the target surface. Due to this the larger particles had lost a more significant fraction of their kinetic energy before impacting the surface, resulting in less damage to the target surface.[5][14] The erosion increases rapidly with grit size up to some critical diameter (50 µm- 100 µm) and then increases at much slower rate or remain constant. This has been attributed to abrasive deterioration and embedding of abrasive with the decrease in abrasive size. When the particle size is less than l µm, wear is no longer caused by the abrasive wear mechanism, but begins to approach the delamination wear. Thus the reason for very small particles being so effective in causing erosion is not at all clear. Thus the reason for very small particles, it has been found that normally brittle materials will erode in a typically ductile fashion.

- **Slurry concentration**

  Many studies on slurry erosion are done by varying slurry concentration. It is observed that erosion due to slurry concentration mainly depended on the type of erodent. The collision efficiency of the slurry decreased when it became more concentrated, although the absolute amount of weight loss increased with increasing slurry concentration.[5][14]

- **Cavitation**

  Cavitation phenomenon also occur during the slurry erosion test. Some researcher used Cavitation inducer to enhance the cavitation for studying the effect of cavitation during slurry erosion test. Amarendra et al. [15] analyzed the combined slurry and cavitation erosion resistance of HVOF thermal spray coated stainless steel and concluded that presence of cavitation inducer increases the material loss.

2.1.4 Slurry erosion in different steels

Lindgren et al. [16] investigated Erosion–corrosion resistance of two austenitic stainless steel grades and three duplex stainless steel grades in high-temperature sulfuric acid solution. They concluded that Erosion–corrosion synergy was not dependent on the stainless steel grade & an increase in the initial test temperature of the erosion–corrosion had a significant impact on mass losses. Kishor et al.[17] investigated Slurry erosion of thermo-mechanically processed 13-Cr-4-Ni stainless steel. They performed the slurry erosion test at 10 wt % slurry concentration at a constant rotational speed of 500 rpm for 24 hrs. They concluded that Microstructure of the TMP steels

evolved into finer martensite lath packets, which improved their slurry erosion resistance. It showed 78% more improvement in the slurry erosion resistance as compared to the ASR 13/4 MSS. Ojala et al. [18] studied wear performance of quenched wear resistant steels in abrasive slurry erosion. They used a pin mill type sample arrangement at two different angles 45 ° and 90°.They concluded that , high-stress abrasive wear becomes dominant when the size of the abrasive particles exceeds 1–2 mm. In These conditions, the quenched wear resistant steels shows comparable wear resistance as compared to elastomers. In the case of low-stress abrasive slurry erosion conditions produced by particles less than 1 mm in size, limited plastic deformation of the steels occurs which further results in lack of work hardening.

Khan [19] performed slurry erosion test on mild steel sample. He used fly ash slurry with different concentration for the test. He concluded that erosion wear increases with increase in slurry concentration with passage of time. The rate of increase in erosion wear is steady from 20% to 40% but after 40% the rate of increase in erosion wear is decreased the ash particles start losing their sharp edges because of this interaction. Dhawan et al. [20] investigated the erosion behaviour of stainless steel grade-316 with different erodent size, concentration and speed. He concluded that erosion increases with the increase in erodent size and speed but with increase of slurry concentration erosion first decreases and then again increases. Ojala et al. [21] performed high speed slurry-pot erosion wear testing of AISI 316 stainless steel samples with large abrasive particle. They concluded that large and sharp particles cause more wear than small and rounded particles. Agarwal et al. [22] Slurry and cavitation erosion of HSLA steel processed by warm multidirectional forging and inter-critical annealing. They performed the slurry erosion test with a relative velocity of 3.5m/s between specimen and, angle of attack of 90°. They concluded that Dual phase HSLA steel showed the best slurry erosion resistance because of negligible micro cutting and low plastic strain from slurry impact. Wood et al. [23] investigated Influence of microstructure on the erosion and erosion–corrosion characteristics of 316 stainless steel. They performed slurry erosion test in both distilled water and 3.5% NaCl w/w in distilled water with the presence of 1%w/w silica sand at a test velocity of 7ms^{-1}. They studied both erosion and erosion-corrosion behaviour of the stainless steel. They concluded that both erosion and erosion–corrosion surfaces shows similar surface features including impact crater, particle embedment and crater lip formation. They also pointed that the synergy rate was higher than that for pure erosion only.

In majority of the cases silica sand is used for slurry erosion tests because of its high hardness and wide availability. Silica is the second most abundant mineral present on earth crust and can be found in form of sand be it deserts, beaches, river beds or sandstones. Because of aforesaid reasons there is high chances that material of interest will face slurry of the silica particles. In the current work silica sand is selected as erodent for the slurry. In the literature researcher performed slurry erosion test with range of particle sizes be it coarse sand or fine sand. In the current work size of erodent is taken as less than or equal to 297 µm.

2.1.5 Wear mechanisms

Different types of wear mechanism are reported in literature during slurry erosion**.** These wear mechanisms are discussed below.

2.1.5.1 Cutting mechanism

Basically, cutting is a mode by which material can be removed from the surface of the bulk material and cutting wear occurs when a hard particle cuts through a softer material. In general, cutting mechanism operates, when the impacting particle contacts the target material at positive rake angle and generates a chip or cut, the material resulting in the generation of new surface.[24] The cutting mechanism is shown in the Fig 6.

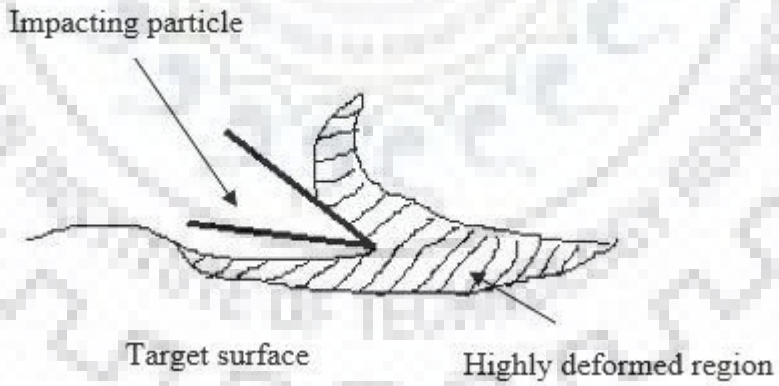

Fig 6: Cutting mechanism [24]

2.1.5.2 Ploughing mechanism

Wear particles in elastoplastic solids are also generated as a consequence of ploughing. Ploughing occurs when material is displaced to the side, away from the wear particles, resulting in the formation of grooves that do not involve direct material removal. When the particle contacts the target work piece at negative rake angles, this mechanism involves the displacement and extrusion of the material with no new surface generation figure 7.The displaced material forms ridges adjacent to grooves, which may be removed by subsequent passage of abrasive particles. Ploughing can generate chips through the formation of ridges which deform and fracture due to subsequent asperity interactions. [25]

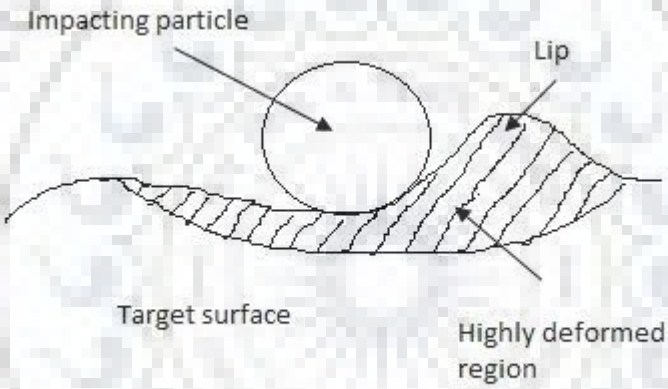

Fig 7: Ploughing mechanism [25]

2.1.5.3 Extrusion and forging mechanism

Evidence that extrusion is the initiation of mechanism of platelet erosion was obtained by Bellman et. al.[26] in their experiment. They described that the loss of material from an eroding surface appears to occur by a combined extrusion forging mechanism. Evidence indicates that the platelets are initially extruded from shallow craters made by the particle impact. Once formed they are forged into a distressed condition, in which they are vulnerable to being knocked off the surface in the form of fragments. [25]

2.1.5.4 Subsurface deformation and cracking

Various investigators [25-27] have shown that by the impact of silt particles, damages are caused in the surface of the target. The subsurface may be deformed by either cutting or ploughing of the material, which may generate chips or wear particles. The wear transition from abrasion to delamination or sliding wear occurs when subsurface deformation, crack nucleation and propagation process can generate wear particles rather than the rate of chip generation. The material at the subsurface undergoes various physical changes when the forces due to the ploughing by wear particles are transmitted from the surface to the bulk.

CHAPTER 3

FORMULATION OF PROBLEM

The basic aim of the study is to analyze the erosion behaviour of ultra-high strength bainitic steel for the potential applications in mining, naval purposes. To analyze the erosion behaviour few parameters (impact angle and duration of erosion) are taken for study. Impact angles varied from 15° to 90° with a step of 15°. To analyze and to characterize the samples for particular duration, every time a new sample is prepared for the erosion test.

For the erosion test, slurry pot erosion tester has been used. In this the samples have been mounted in between the disc plates which were clamped by four bolts. Samples rotated in the slurry at a impact angle adjusted in the sample holder. In the slurry the concentration of the sand particles is 5 wt % and according to the weight loss per hour, the erosion rate is determined.

CHAPTER 4

EXPERIMENTAL PROCEDURE

4.1 Sample preparation

For the study of erosion wear in slurry pipe ultra-high strength bainitic steel samples is used. Specimen dimension is shown in Figure 8. The thickness of the sample was 3mm.

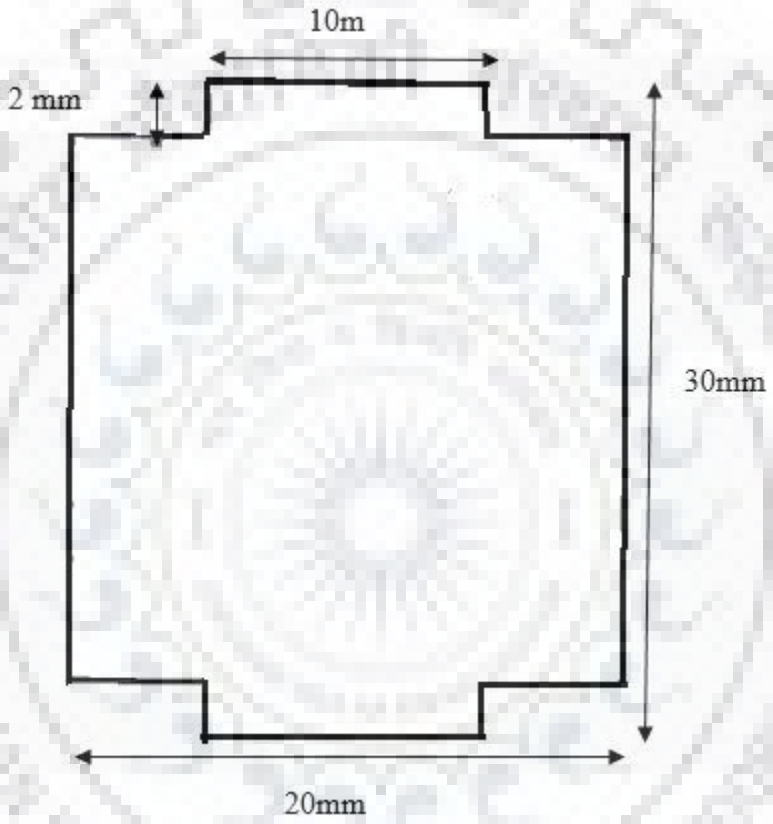

Fig 8: Dimensions of the test specimen

4.2 Steps for microstructure determination

Following were the steps for the preparation of the sample.

1. Sample was polished with the series of emery paper up to 1500 grit size paper

2. Then this sample was cloth polished with the help of cloth polishing machine using water and alumina powder. .

3. Etching has been carried out by using Le Pera reagent (1 wt. % aq. solution of sodium metabisulfite ($Na_2S_2O_5$) to a freshly prepared solution of 4 wt. % picric acid ($C_6H_2(NO_2)_3OH$) in ethyl alcohol, in a 1:1 vol. ratio) as the etching reagent.

4. The polished and etched sample was examined under the microscope.

4.3 Slurry pot erosion test

4.3.1 Description of slurry pot erosion tester

The slurry pot erosion tester consists of a rotating spindle, cylindrical pot which had four baffles that were used to break the slurry flow during testing. Specimen holder was fastened to the spindle of the tester through a connecting rod. The spindle was driven by the motor at 492 rpm. A picture of Slurry pot erosion tester and specimen

Fig 9: Slurry pot erosion tester

holder used for the test is shown in Figure 9 and 10. The schematic top view of the sample holding disc can be seen in Figure 11. After each cycle of erosion testing for given duration, specimen

were washed and ultrasonically cleaned with acetone and then dried with drier before measuring the weight loss.

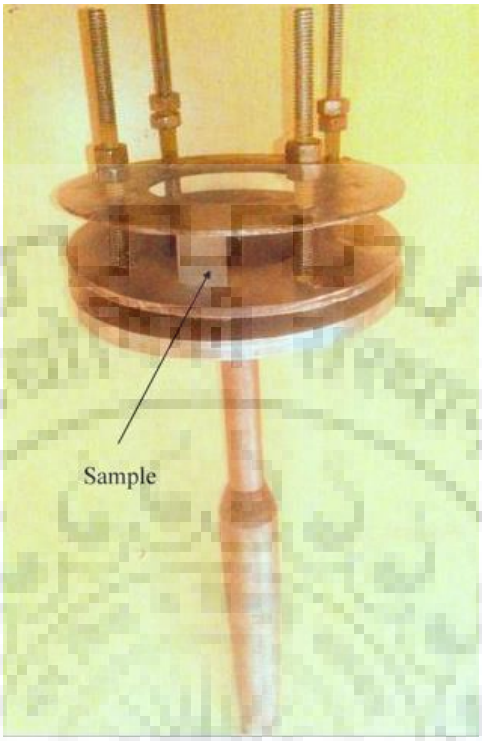

Fig 10: Specimen holder of slurry pot erosion tester

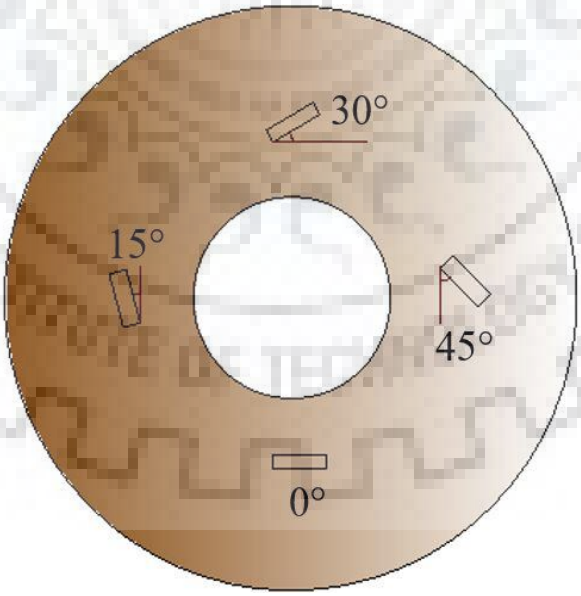

Fig 11: Schematic top view of the sample holder showing different impact angles

4.3.2 Test conditions and parameters

Natural silica sand is used as the erodent with particle size less than and equal to 297 μm. The

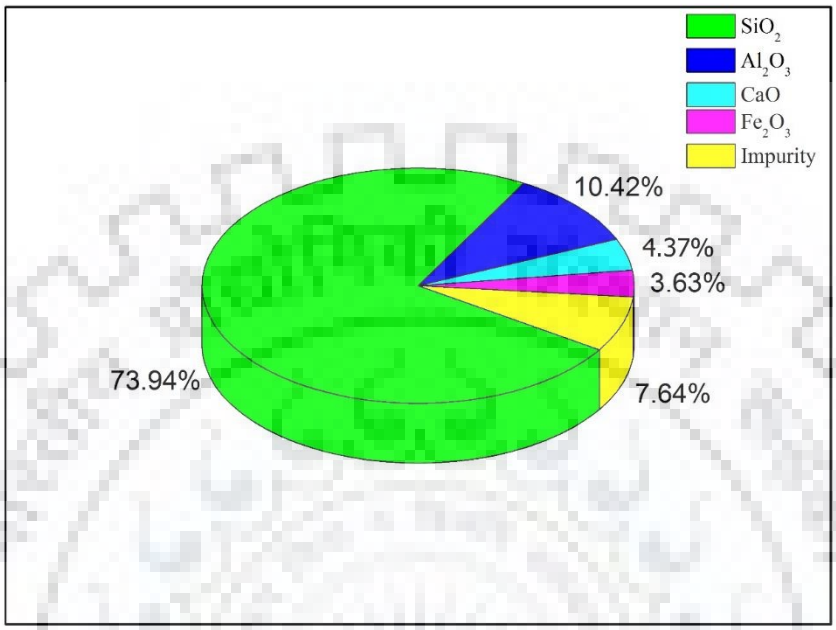

Fig 12: XRF Results of sand used

XRF result of sand used is shown in Figure 12. Figure 12 shows that 73.94 % silica sand is present whereas 10.42 % alumina is present in the sand sample. Sand particles were sieved on Tyler testing sieves in a sieve shaker machine to obtain the size ranges of interest in the experiment. The sieves were arranged as a column one over other .The coarsest meshing at the top and the finest at the bottom with gradually decreasing size of meshing. Sand was kept in the first sieve which had the coarsest meshing. It was made to shake the entire sieve so that the sand settles down in the sieves of different meshing. The desired size of the sand was obtained at the bottom pan of the sieve arrangement.5 wt % slurry concentration is taken for the experiment. Tap water is used as slurry medium. Slurry erosion tests are performed for the duration of 3 hour, 6 hour and 12 hour. Rotational speed of shaft connected to the specimen holder is 492 rpm.

4.3.3 TESTING METHOD

Most of the operations performed in the slurry erosion test are manual. All observations of the experiments were recorded. The sequence of the test operations was given briefly below:

l. The specimen was prepared for the erosion test with the help of the belt grinder and polished on the emery paper.

2. Cleaning the specimen with acetone.

3. Drying the specimen.

4. Prepare the slurry in the container by adding water and sieved sand.

5. Clamp the specimen in the sample holder at different position.

6. Attach the sample holder to the spindle, immerse it in the slurry and lock the spindle.

7. Start the machine and note down the time for operation.

8. Remove the specimen from the spindle and sample holder after erosion testing for desired hours.

9. Cleaning and drying the specimen.

10. Weighing the specimen.

4.4 Scanning electron microscopy

Scanning electron microscopy is used to analyze the worn out surface. FE-SEM QUANTA 200 FEG from FEI as shown in Figure 13, is used for surface analysis of the samples.

Fig 13: Scanning electron microscope used for surface analysis of the sample

4.5 Microhardness measurement

Cross-section of the sample was cloth polished before the micro-hardness test. Micro hardness test was performed in a Omnitech micro hardness tester as shown in Figure 14. Micro hardness was measured in a Vickers scale. 100g load is applied for the microhardness measurement.

Fig 14: Microhardness tester used in the present study

4.6 X-ray Diffraction

Xray diffraction profile for a range of angle 2θ provides quantitative information about the crystallographic feature like crystallite size, strain etc.. Analysis of X-ray line broadening can be done by plotting Williamson hall plot and modified Williamson hall plot.

3.6.1 Williamson-hall plot

Williamson hall equation [28] can be written as following as shown in equation (1)

$$\beta Cos\theta = \frac{0.9}{D} + 4\epsilon \, Sin\theta \ldots\ldots\ldots\ldots\ldots\ldots \text{(1)}$$

Where β =FWHM of the peak = $\beta_{measured} - \beta_{instrumental}$

λ= Wavelength used in XRD

ϵ = strain

$\beta_{instrumental}$ can be calculated by obtaining XRD spectra of standard strain-free material (LaB_6 , Al_2O_3 or Si) from the same instrument and then measuring the FWHM of the peaks obtained. In this study standard strain-free crystals of Si were diffracted in the same instrument over a 2θ range of 30-120 in order to measure the instrumental broadening as shown in Figure 15. Peak broadening of the peaks calculated from the XRD spectra. This peak broadening is subtracted from the peak broadening of the XRD spectra of the ultra-high bainitic steel.

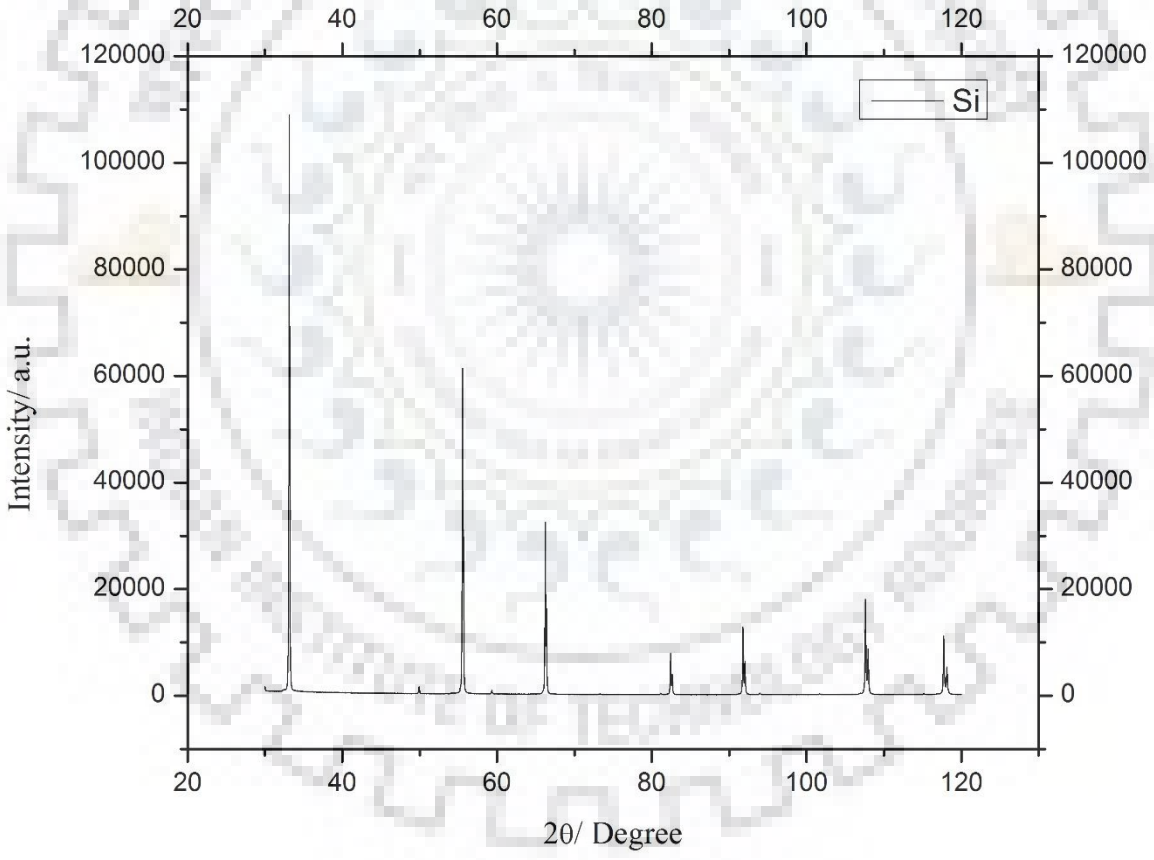

Fig 15: X-ray diffraction profile of strain free pure Si crystals used for the calculation of instrumental broadening of the diffractometer

By plotting βcosθ vs sinθ from equation (1), we can find out crystallite size D and strain ε from the intercept and slope of the linear regression line. Further dislocation density is calculated form the Williamson and Smallman equation [29] as given below:

$$\rho = \frac{\sqrt{12\epsilon}}{bd} \text{.....(2)}$$

Where ρ = Dislocation density

ϵ = strain

b= burgers vector

d= interplanner spacing.

Magnitude of the burgers vector can be calculated as by given formula below:

$$\text{b} = \frac{a}{2}\sqrt{(h^2 + k^2 + l^2)} \text{..... (3)}$$

where, a = lattice parameter

For face-centered cubic structure b is given by $\frac{a}{2}$<110>, thus magnitude of this burgers vector is given by,

$$\text{b} = \frac{a}{\sqrt{2}}$$

4.6.2 Modified Williamson-Hall plot

For anisotropic materials , the linear regression line of Williamson hall plot bears a poor correlation with the experimental data, which would lead to an erroneous calculation of the crystallite size (D) and lattice micro-strain (ε) as detailed by Ungar and co-workers.[30-33]

Modified Williamson hall equation [32] can be written as following as shown in equation (4):

$$\Delta K = \frac{0.9}{D} + \sqrt{\frac{\pi M^2 b^2 \rho}{2}} K\sqrt{C_{hkl}} + \text{O}\,(K^2 C_{hkl}) \text{..... (4)}$$

Where, D is the size parameter, k equals to 0.9, ρ and b are the average dislocation density and the length of the Burgers vector of dislocations. M is a constant defined as the outer cut-off radius of dislocations and O stands for the higher order terms in ${K^4 C^2}_{hkl}$. C_{hkl} is the average dislocation contrast factor for a specific hkl plane. The value of M generally varies from 1 to 2 and it depends

upon amount of deformation of the material. In the present study value of M is assumed to be 1.5 for the calculation of dislocation density.

$$\Delta K = \frac{\beta Cos\,\theta}{\lambda}$$

$$K = \frac{2Sin\theta}{\lambda}$$

For fcc and bcc lattices, the average contrast factor for a particular Bragg reflection hkl, C_{hkl}, can be calculated from the contrast factor of h00, C_{h00} as explained in [32];

$$C_{hkl} = C_{h00}(1\text{-}qH^2) \quad \text{..... (5)}$$

Where, C_{h00} is constant corresponding to the elastic properties of the microstructure [32]. For fcc and bcc lattice, H can be expressed as,

$$H^2 = \frac{(h^2k^2+k^2l^2+l^2h^2)}{(h^2+k^2+l^2)}$$

and q, is the parameter corresponding to the type of dislocations and its numerical value changes with the change in fraction of edge and screw dislocations in the microstructure. The value of C_{h00} and q parameter can be obtained Ungar et.al.[32]

CHAPTER 5

RESULTS AND DISCUSSION

5.1 Optical micrograph

The microstructure of the as received specimens have been studied. The polished and etched sample was examined under the Lieca microscope. Optical micrograph of the sample is shown in Figure 16. Optical micrograph clearly shows the region of retained austenite and bainite. White region is the region of retained austenite whereas blue region is the region of bainite. Few amount of martensite is also observed as shown in optical micrograph with brownish region.

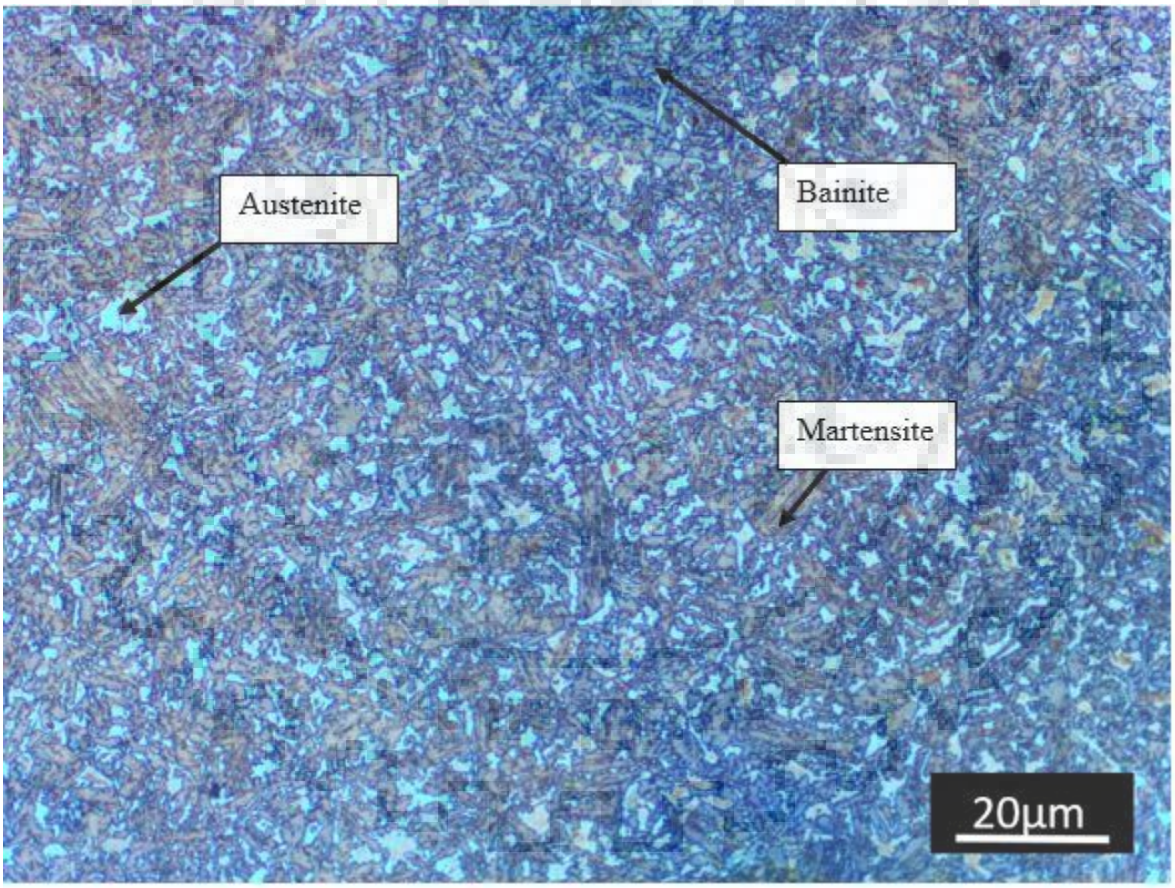

Fig 16: Optical micrograph of the as-received ultra-high strength bainitic steel sample showing presence of different microstructural constituents

5.2 Test results

Weight loss of specimens after slurry erosion tests were measured by using an electronic micro balance with 0.01 mg resolution. Wear rate of the samples for 3 hour, 6 hour and 12 hour is plotted against different impact angles as shown in Figure 17.

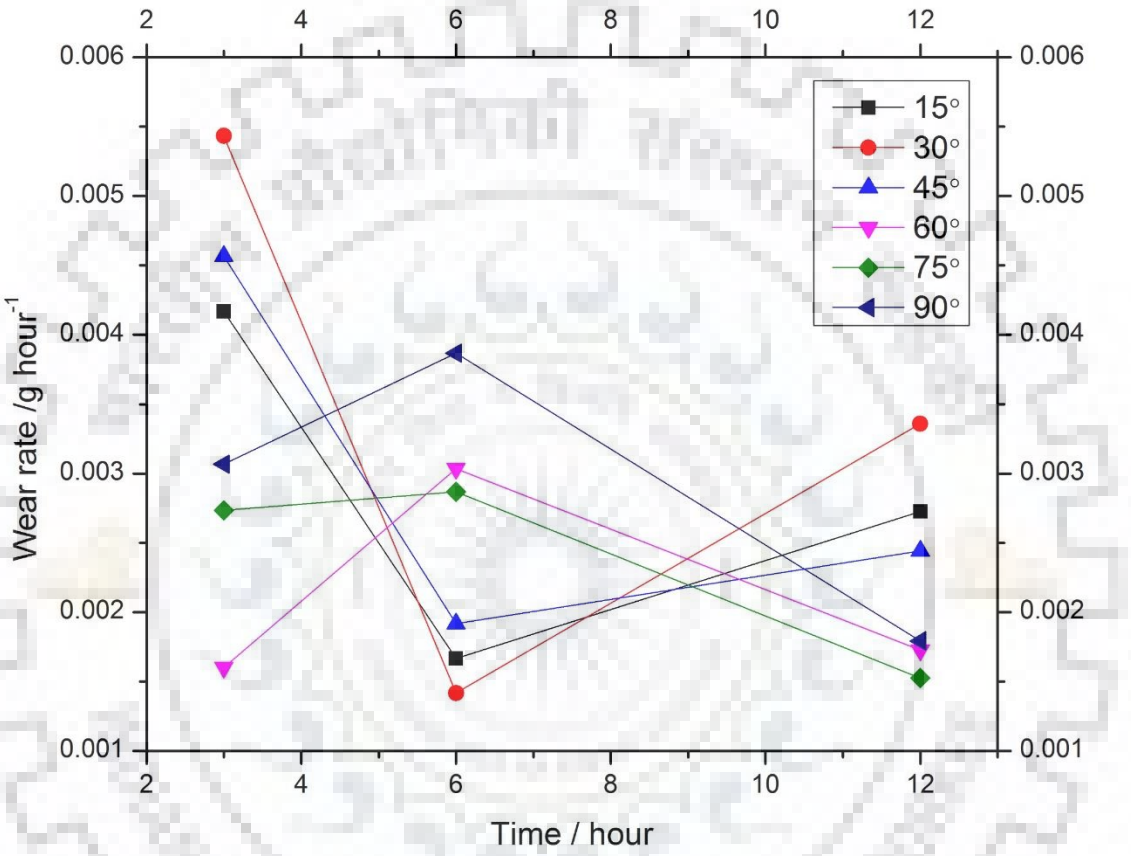

Fig 17: Wear rate of the samples with erosion time at different impact angles

The above figure shows two different trends for low impact angles (15-45) and for high impact angles (60-75). This shows that there is effect of impact angles on the wear rate of the ultra high strength bainitic steel. To further investigate the reason behind this trend SEM analysis is done and it is discussed in the next section.

5.3 Scanning electron microscope Analysis

After the erosion test of 3h, 6h and 12hr, SEM images of the samples for different impact angles and the SEM images of the sand used were taken. These images are analyze to investigate the worn out surface and wear rate of the material.

5.3.1 Effect of impact angles

Figure 18 (a), (b) and (c) shows SEM images of samples which were put at the low impact angles. SEM images clearly show that there are erosion pits which were non-circular elongated shape. SEM images of samples at high impact angles shows more of circular craters and worn out spots. These two types of erosion pits are due to two different type of mechanisms at low impact angles as compared to the high impact angles. At low impact angles the erodent particle will tend to rub the surface so the elongated erosion pits will present as can be seen in the Figure 18 (a), (b) and (c).

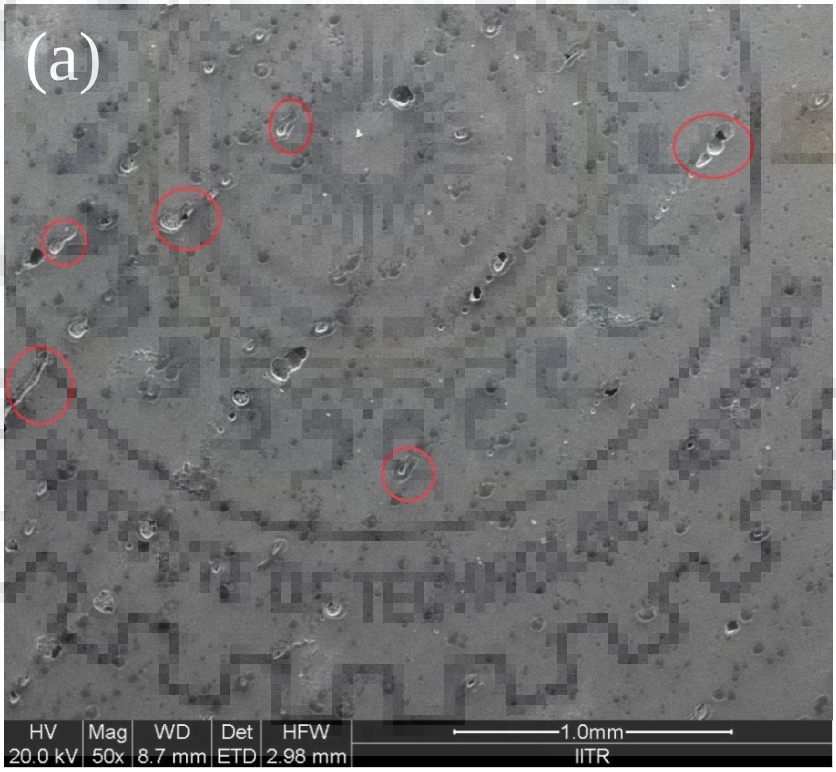

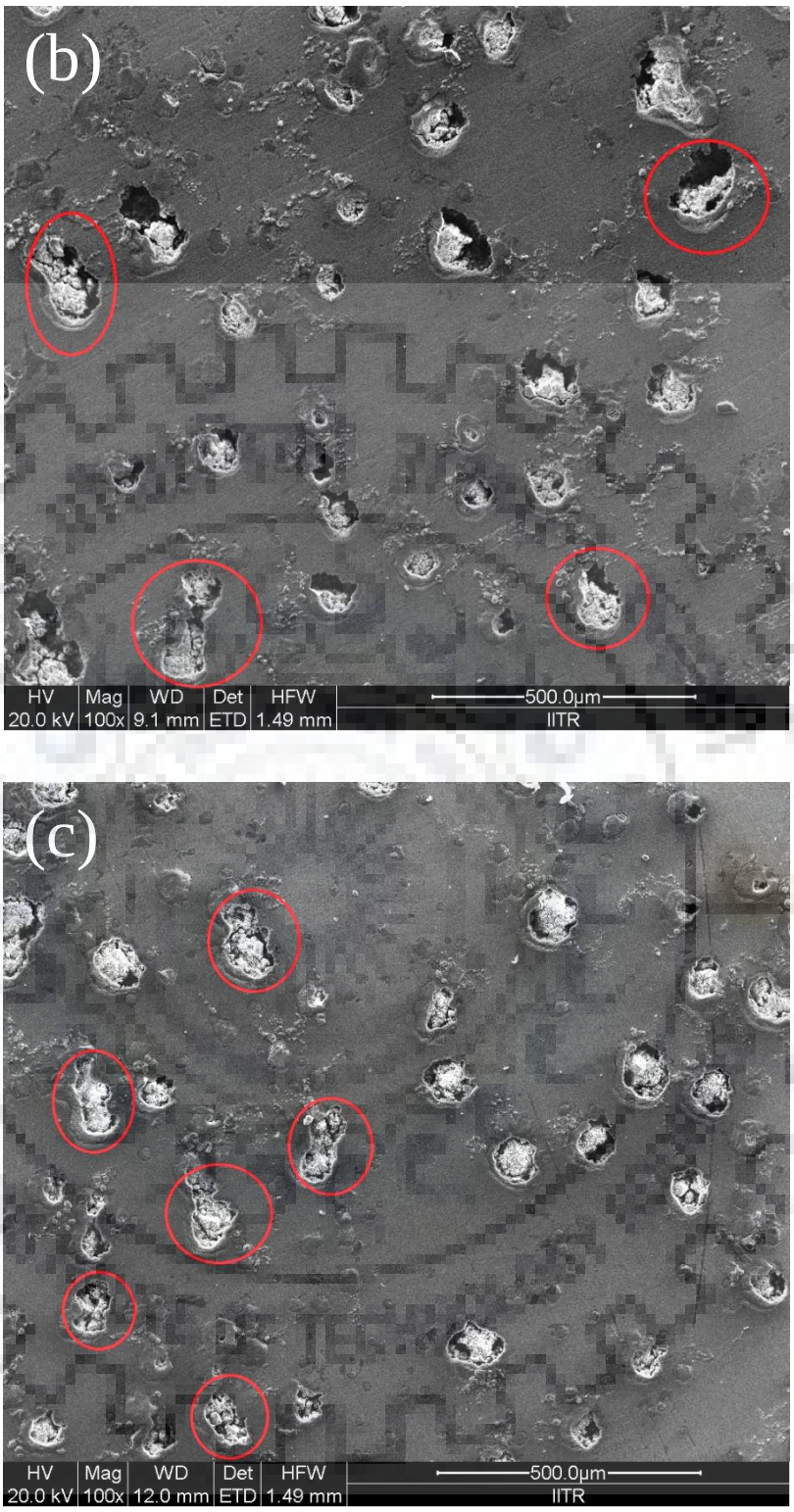

Fig 18: SEM image of the surface of the samples after erosion testing of (a) 6 hour at 15° impact angle (b) 12 hour at 15° impact angle (c) 12 hour at 45° impact angle

At high impact angles the SEM images shows more circular erosion pits as shown in figure 19(a), (b) and (c). The reason for these types of erosion pits is that at high impact angles erodent particle will directly hit the surface and there will be low amount of rubbing with the surface. The nucleation of micro-cracks will happen with further particle strikes. These micro crack will propagate along the impact direction and will go deeper in the surface.

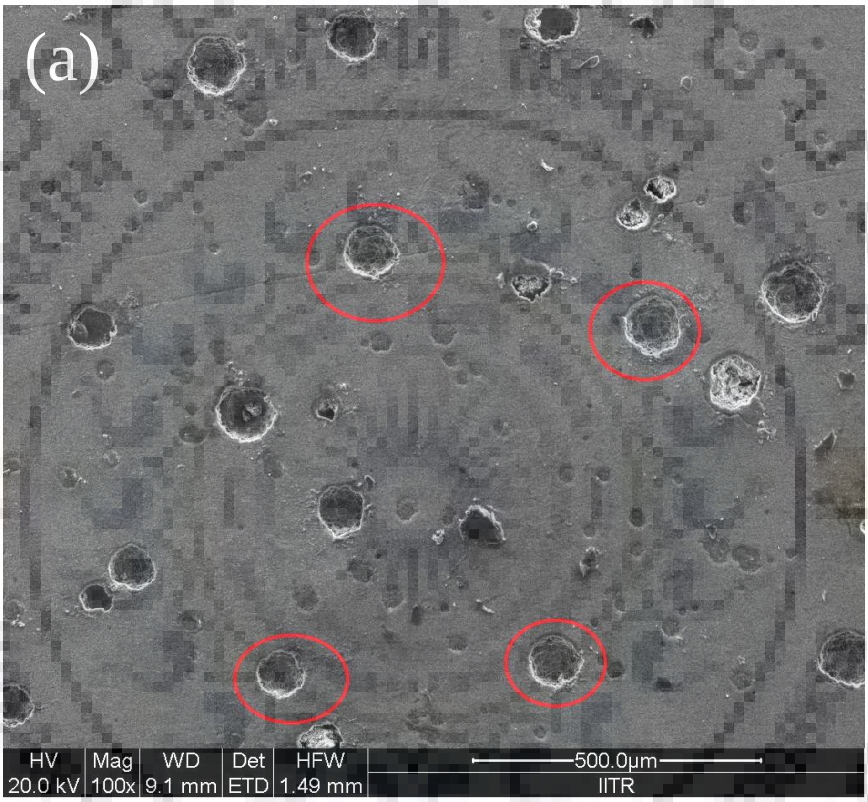

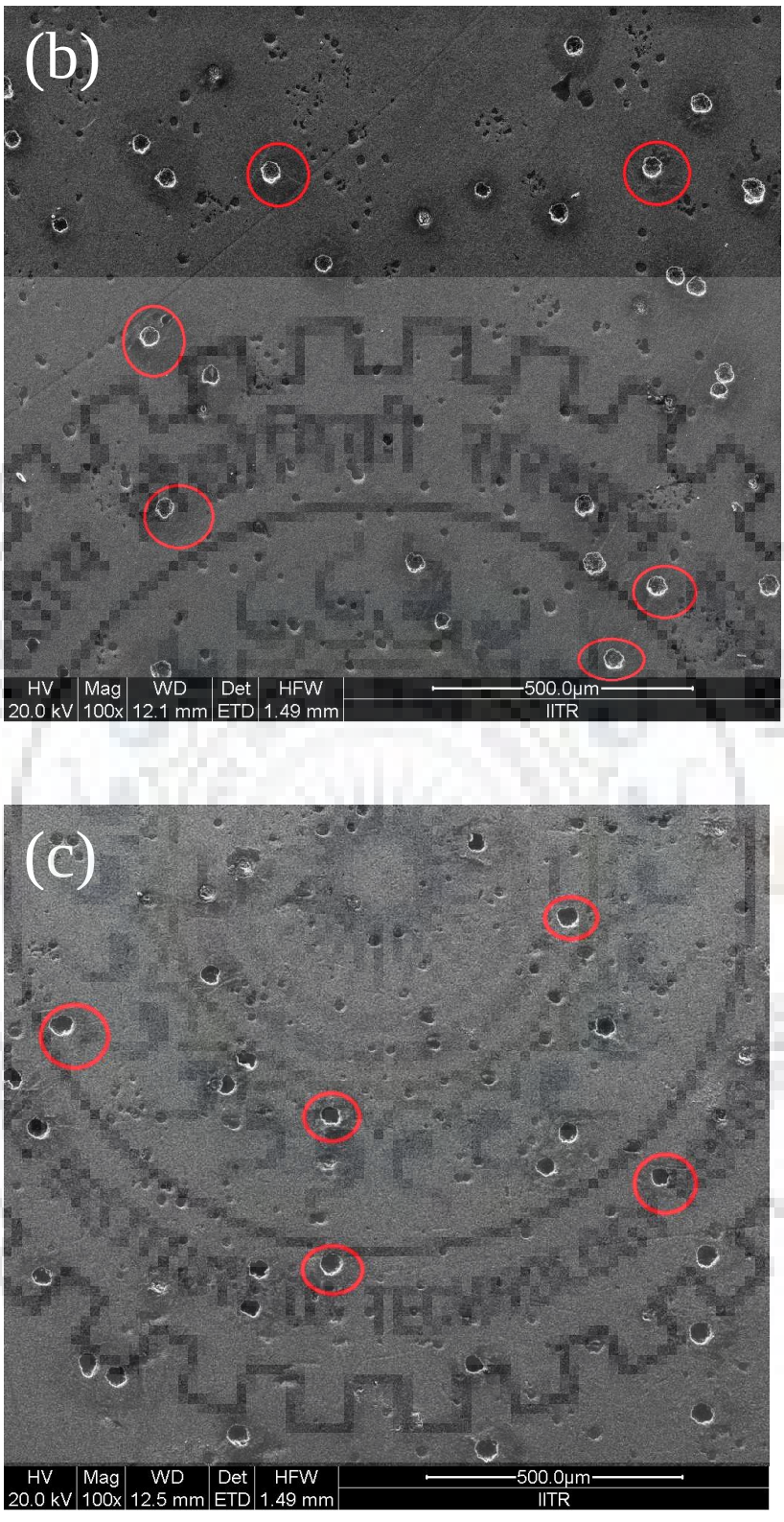

Fig 19: SEM image of the surface of the samples after erosion testing of (a) 12 hour 90°impact angle (b) 6 hour at 75°impact angle (c) 6 hour at 90° impact angle

5.3.2 Depth of erosion pits

Further SEM images of the cross section of the samples of different duration were analyzed to

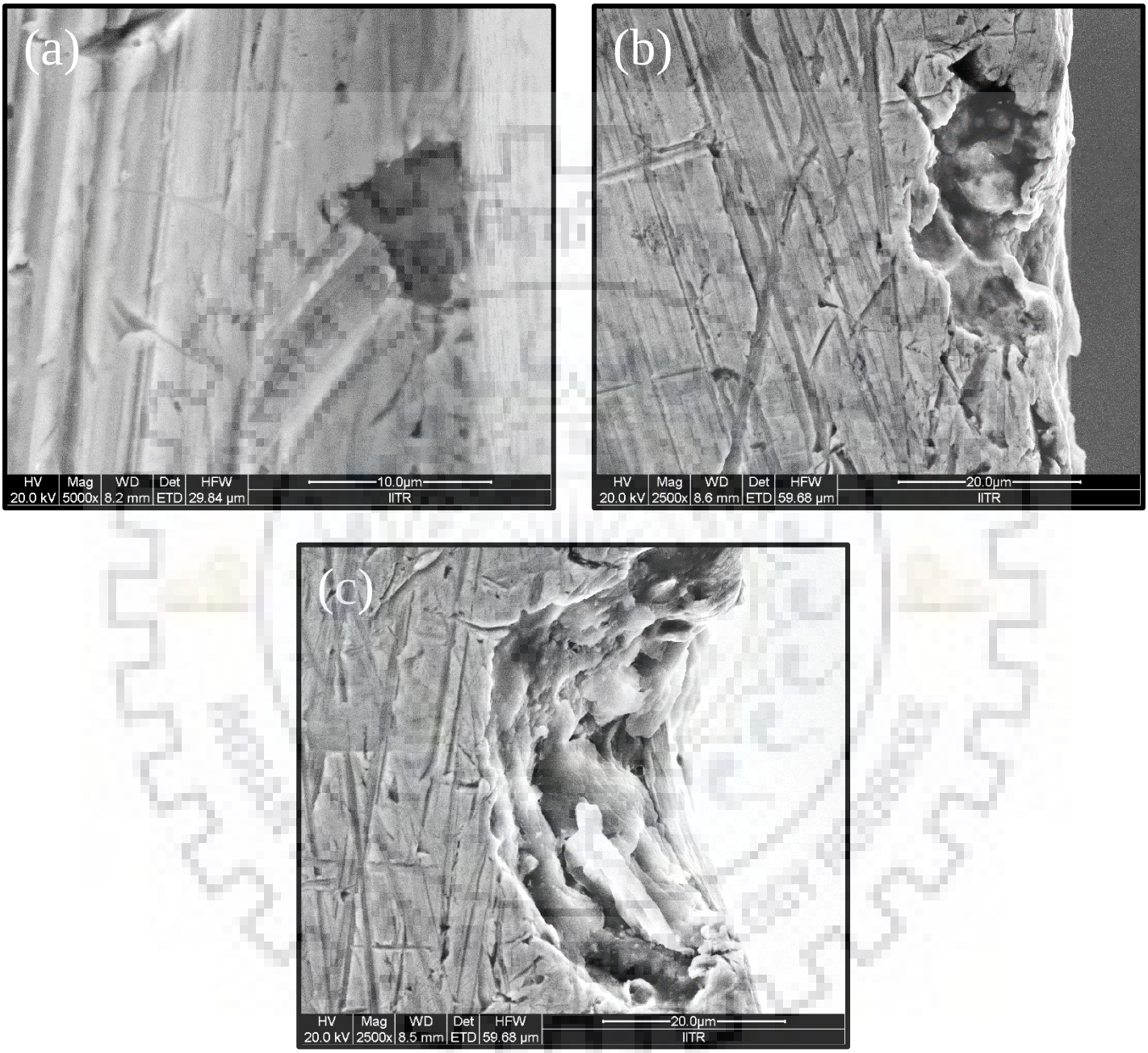

Fig 20: SEM image of the cross section of the samples after erosion testing of (a) 3hr, (b) 6hr (c) 12hr

get the information about the depth of erosion pits. Fig. 20 (a), (b) & (c) shows the SEM images of cross-section of erosion pits of samples of 3hr, 6hr and 12hr erosion testing. Depth of erosion

pits is measured from the SEM images by the “Image J” software by taking the scale given in the SEM images. The average value of depth of erosion pits is plotted against the erosion time in figure 21. Figure 21 shows that average depth of erosion pits is increases with erosion time

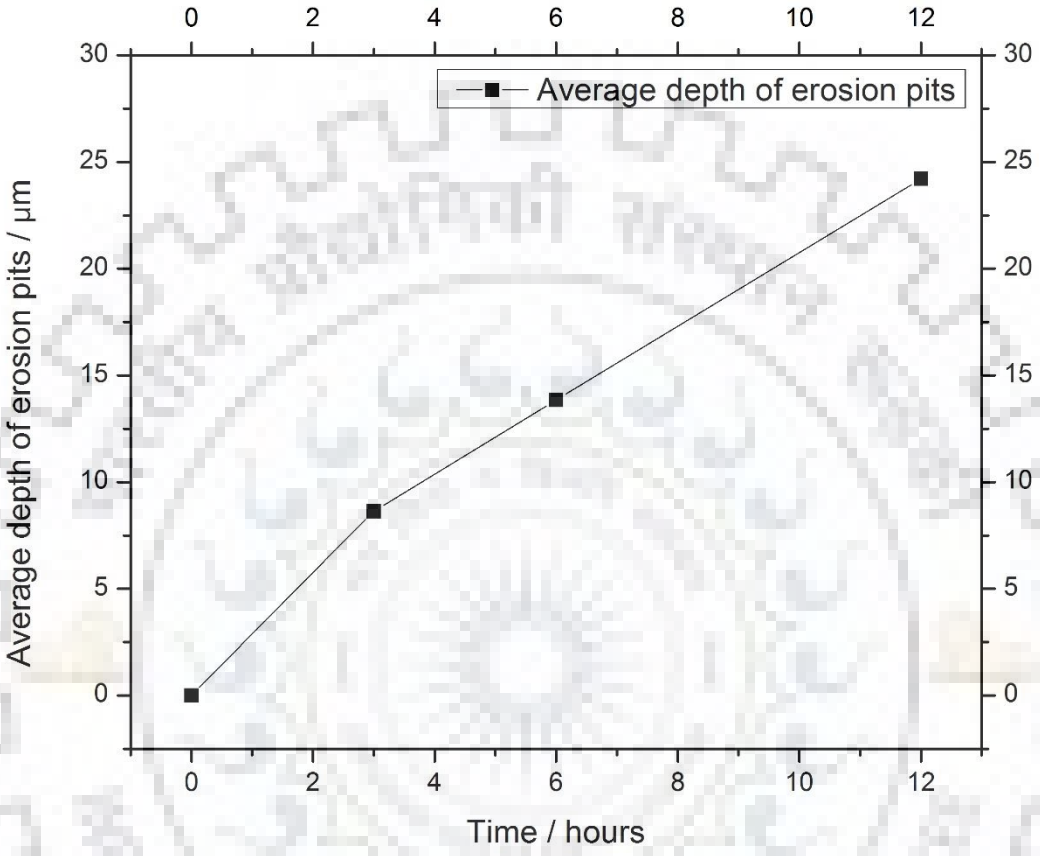

FIG 21: Depth of erosion pits from the surface of samples

The increase in average depth of erosion pits with erosion time shows that micro-cracks propagates deeper in the surface and chipping-off of the fragments of material occurred continuously with further particle strikes.

5.3.3 Wear mechanism

SEM images of the erosion pits are shown in Figure 22. These images shows formation of erosion pits. Figure 22 (a) & (b) shows shat micro-cracks forms during the initial stages of the erosion. Figure 22 (c), (d) & (e) suggests that these micro-cracks propagate in the direction of impact and went deeper in the subsurface. Small chunks of material is continuously getting removed during the next stages of the erosion.

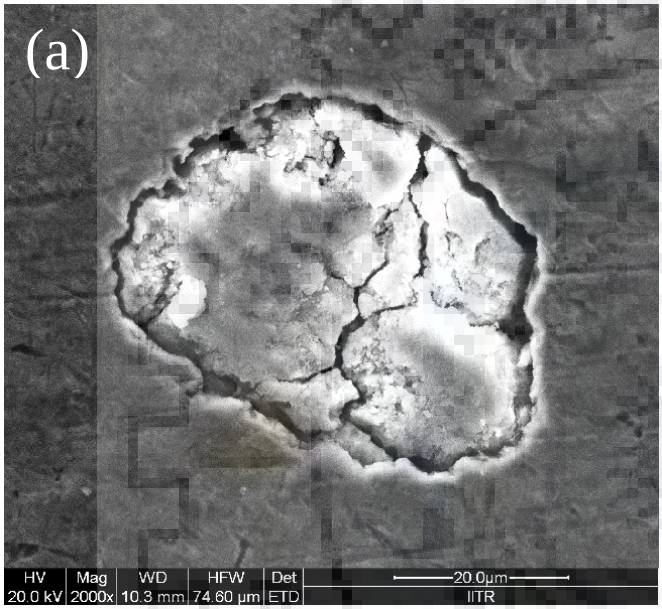

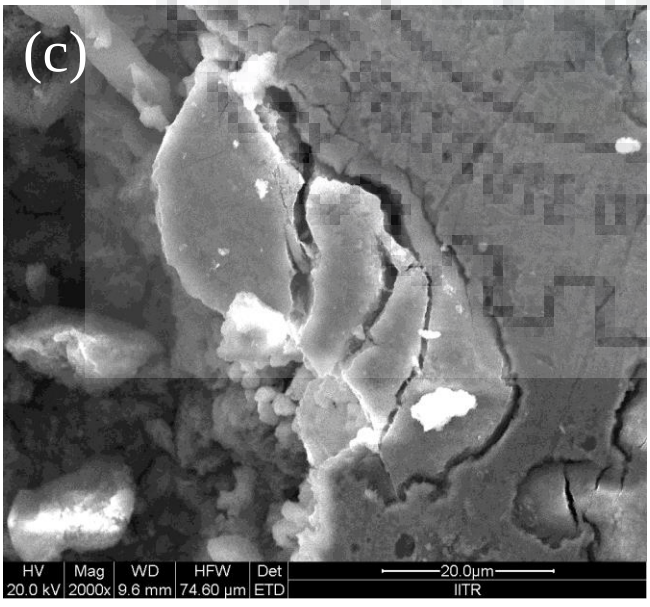

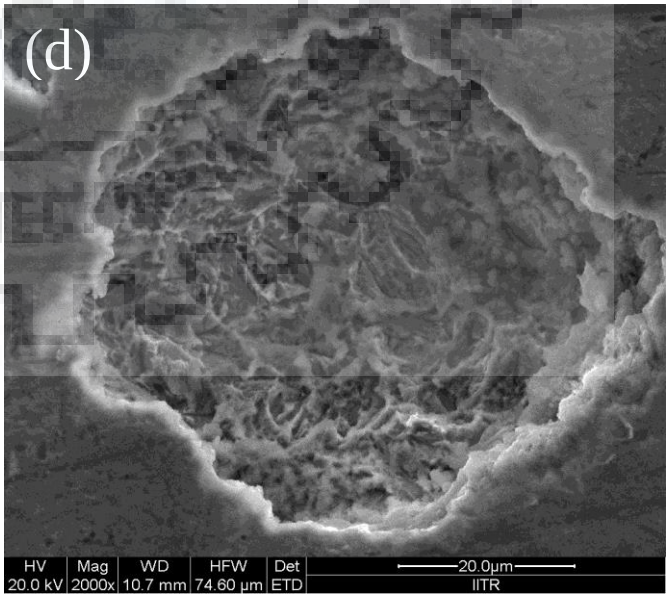

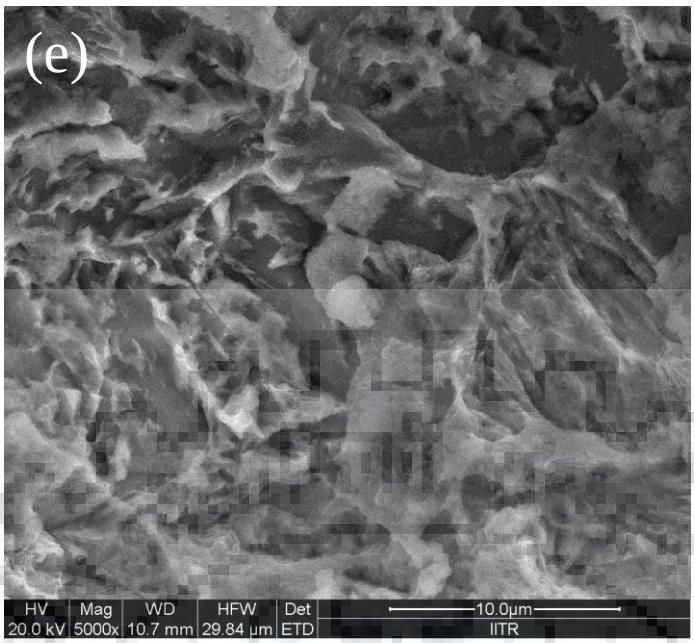

Fig 22: SEM images of the erosion pits of the samples after slurry erosion (a) initial stage of formation of erosion pits (b) micro cracks on erosion pits (c) fragments of material chipping-off from the pit (d) erosion pit after fragments of material got removed (e) zoomed view inside the erosion pit

Thus micro crack propagation in the direction of the impact is the major wear mechanism of the ultra-high strength bainitic steel irrespective of impact angle. The only difference between samples after erosion testing at low impact angles and high impact angles was shape of erosion pits. The zoomed view inside the erosion pit as shown in Figure 20 (e) shows that material is removed in the form of small chunks of material.

5.3.4 Sand particles shape analysis

SEM images of sand used after slurry erosion is taken to analyze the sharp edges of the sand particles with duration of time. Figure 23 (a), (b) &(c) shows that sand after the test due to sand- sample material and sand-sand interaction, particles start to lose their sharp edges as shown in Figure 23. The sharp edges of the erodent particle became blunt. Due to this reason change in wear mechanism occurs. In the initial stages cutting mechanism dominates and when the sharp edges of the erodent particle become blunt ploughing and subsurface cracking mechanism dominates. This shift in wear mechanism can be seen in wear rate results.

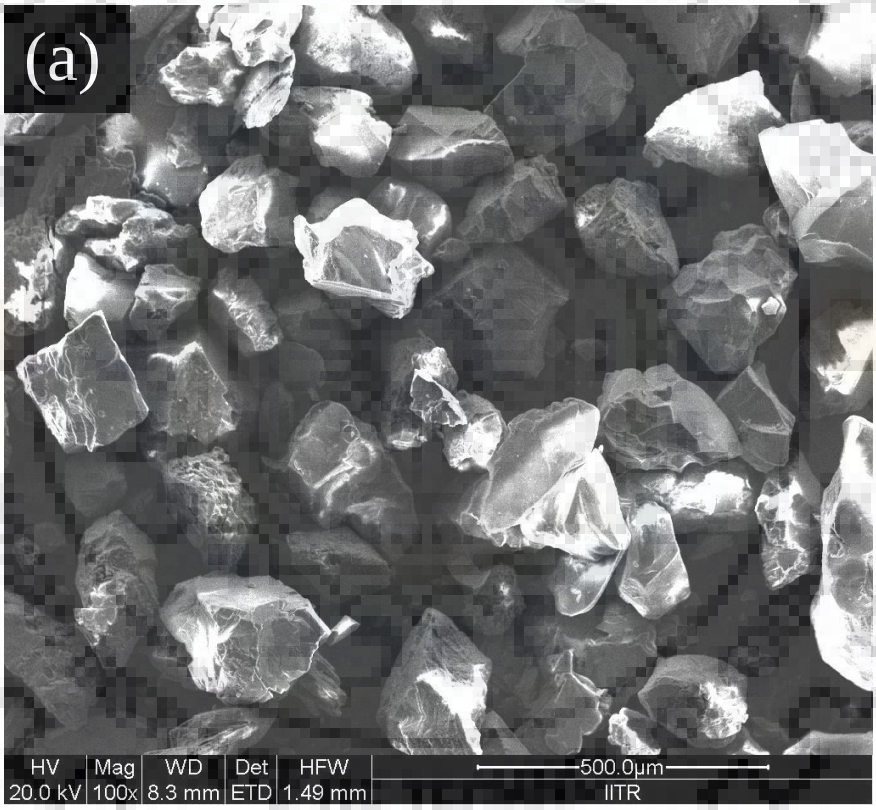

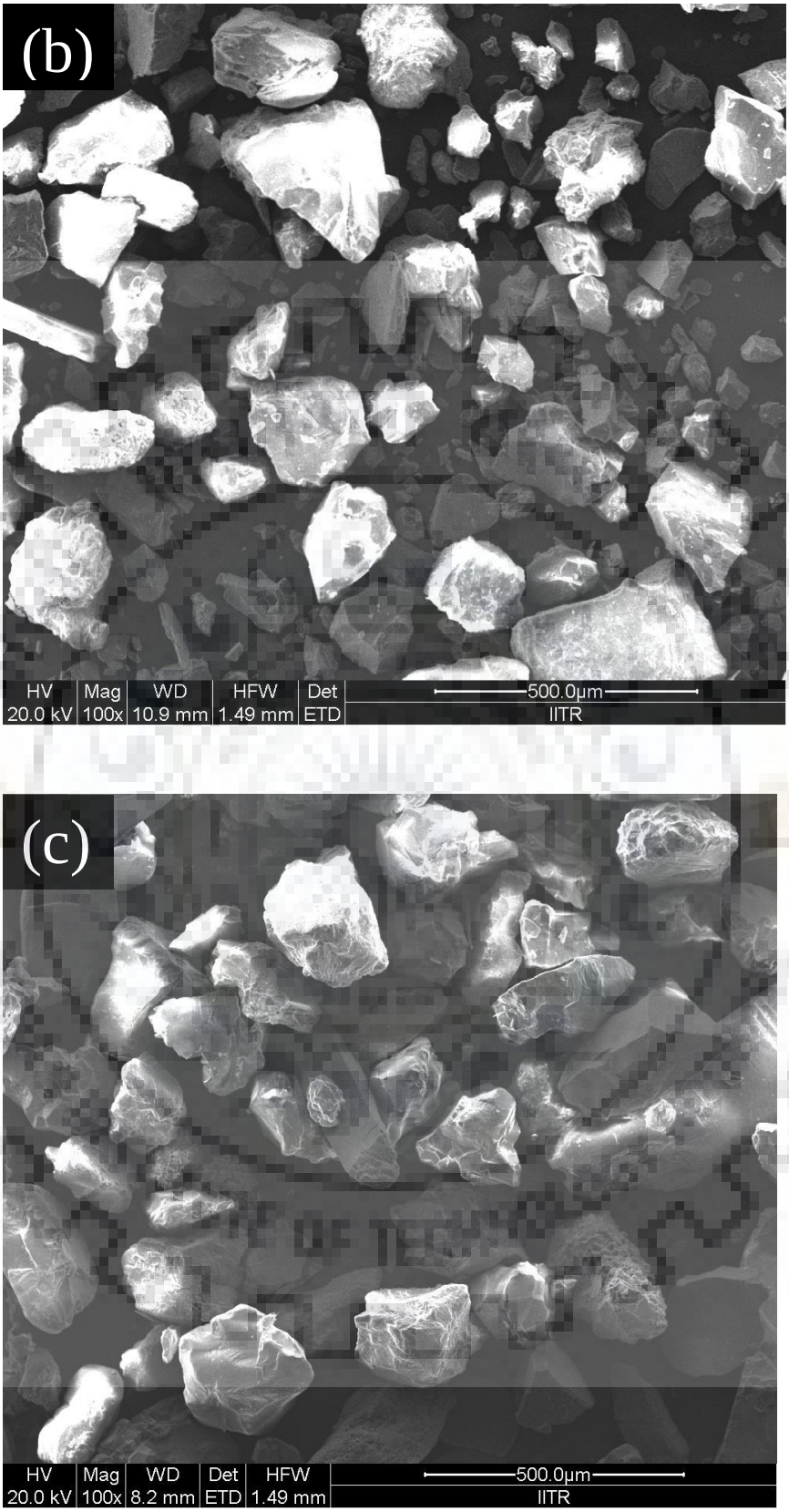

Fig 23: SEM images of sand used after slurry erosion (a) 3hr (b) 6 hr (c) 12 hr

5.4 Microhardness measurement

Cross-sections of the samples after erosion testing of 3hr, 6hr & 12hr are analyzed. Micro hardness was measured on the cross section near the eroded surface. Micro hardness results are shown in Figure 24. Micro hardness profile shows that there is a marginal increase in hardness after erosion testing of a 6 hr but significant increase in hardness after 12hr erosion testing. This shows high amount of subsurface deformation in the sample after 12hr erosion testing.

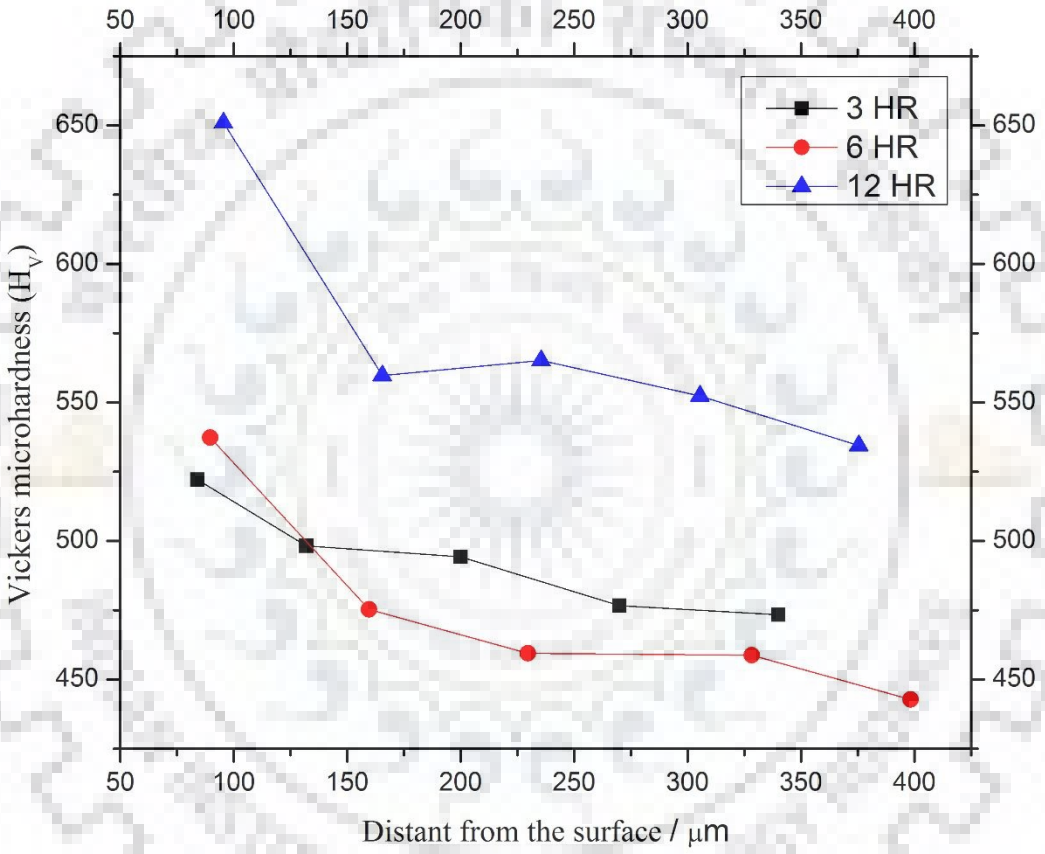

Fig 24: Microhardness profile of the cross section of the samples after erosion testing of 3hr, 6hr, 12 hr

The increase in the hardness of subsurface region suggest the possible phase transformation of retained austenite to deformation induced martensite.

5.5 XRD Analysis

XRD Analysis is done to characterize the samples obtained after erosion testing. The XRD of as received sample is given in Figure 25. The Figure 25 show the positions of peaks of austenite and ferrite with respective hkl values. The major focus of xrd analysis is on the retained austenite phase present in the base material as to investigate the possibility of phase transformation of retained austenite into untampered martensite. To analyze this phase fraction of austenite is calculated for all the samples after the erosion test and it is discussed in the next section.

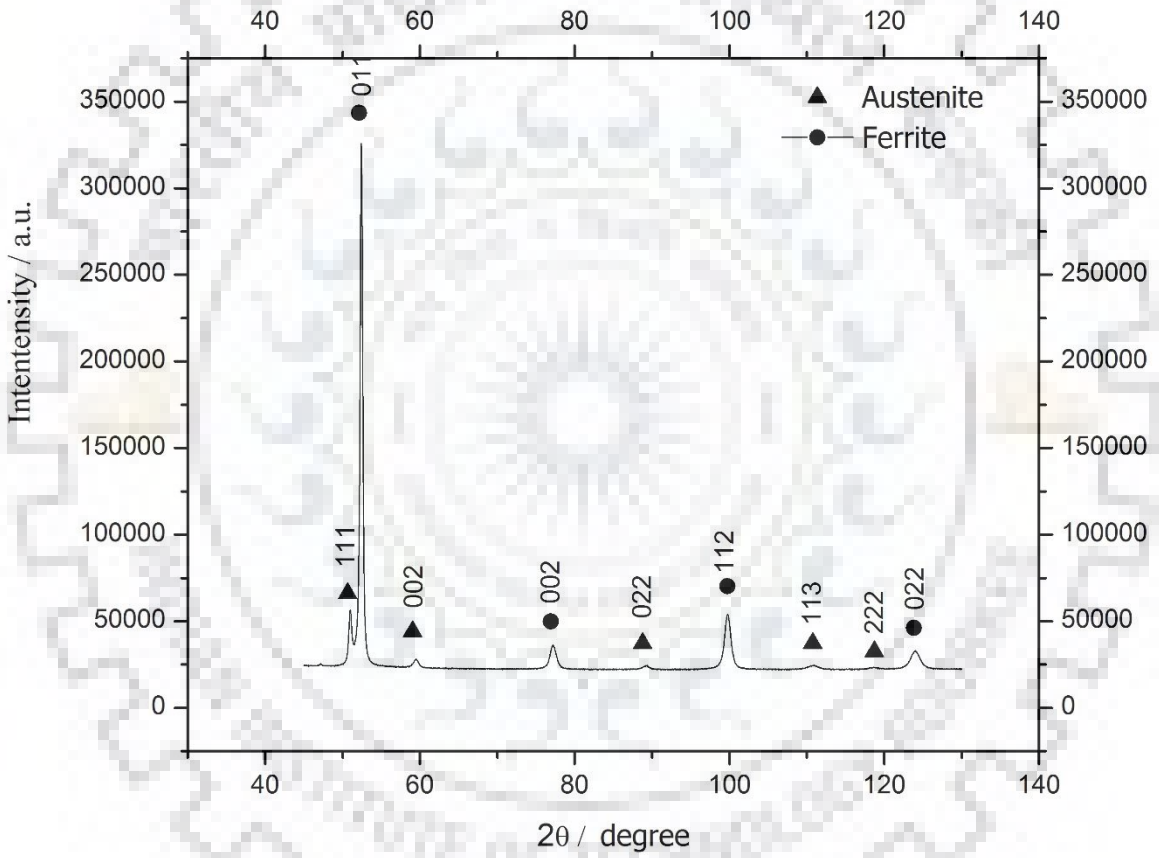

Fig 25: XRD profile of as received sample of ultra-high strength bainitic steel

5.5.1 Quantitative phase analysis

Phase fraction can be calculated for analyzing the austenite phase. After the acquisition of the spectra, the Rietveld analysis was carried out in MAUD software. A series of iteration and refining of several parameter is carried out to reasonably good match between I^{exp} and I^{cal} with low Goodness of fit values. Figure 26 shows the observed and calculated values of intensities of the XRD spectra of the as received sample. Likewise rietveld analysis was carried out for the XRD spectra of the all samples after the erosion testing of 3hr, 6hr, and 12hr with different impact angles.

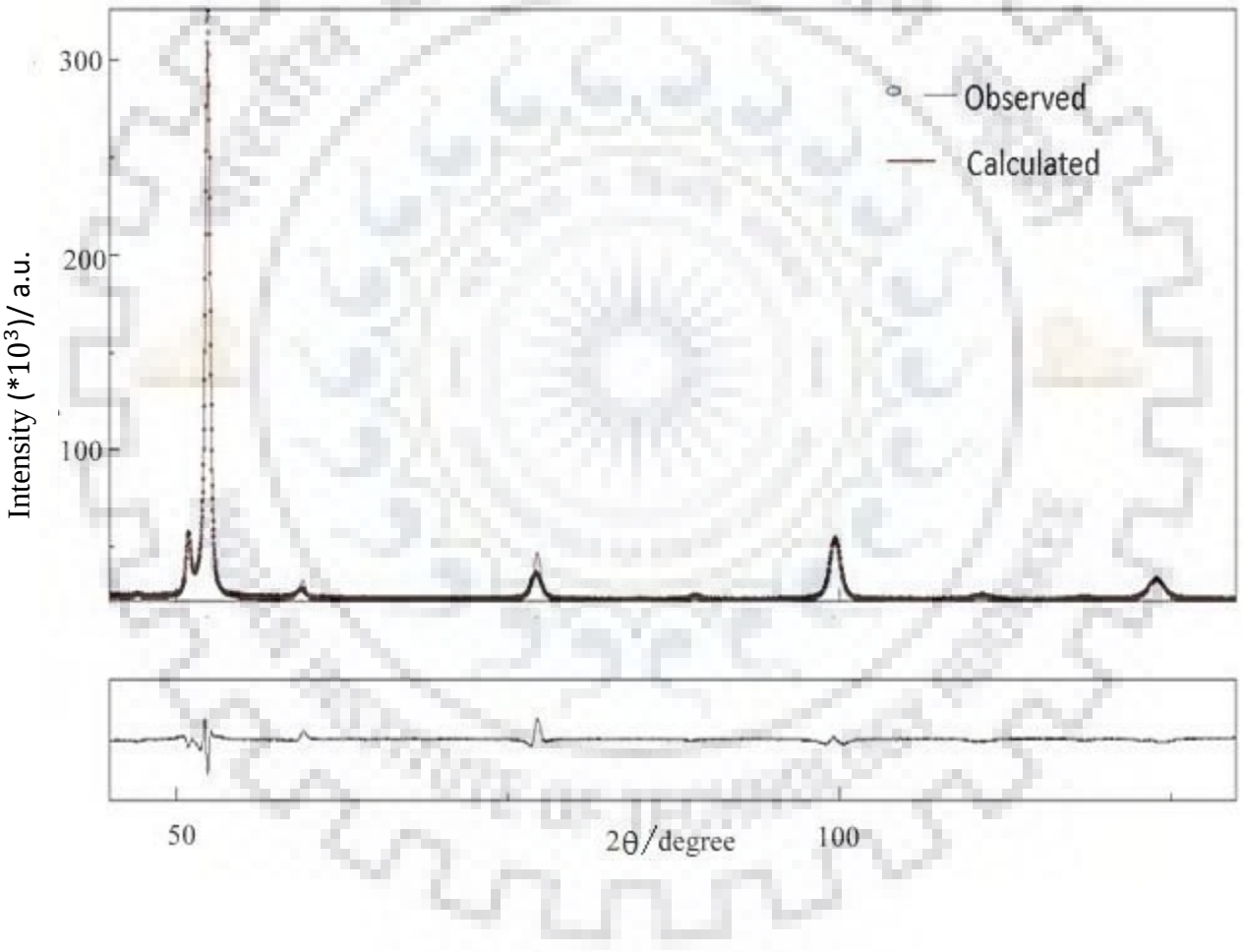

Fig 26: Observed and calculated values of intensities of the XRD spectra of the as received sample

Phase fraction analysis shows a similar trend for all the samples as shown in Figure 27. Figure 27 shows that fraction of retained austenite is decreasing for 3hr duration and then slightly increases and again decreases. The decrease in austenite phase fraction hints the possibility of deformation induced phase transformation of retain austenite into the martensite phase. This marginal increase and decrease in austenite phase fraction was occurred because material removal also taking place from the surface.

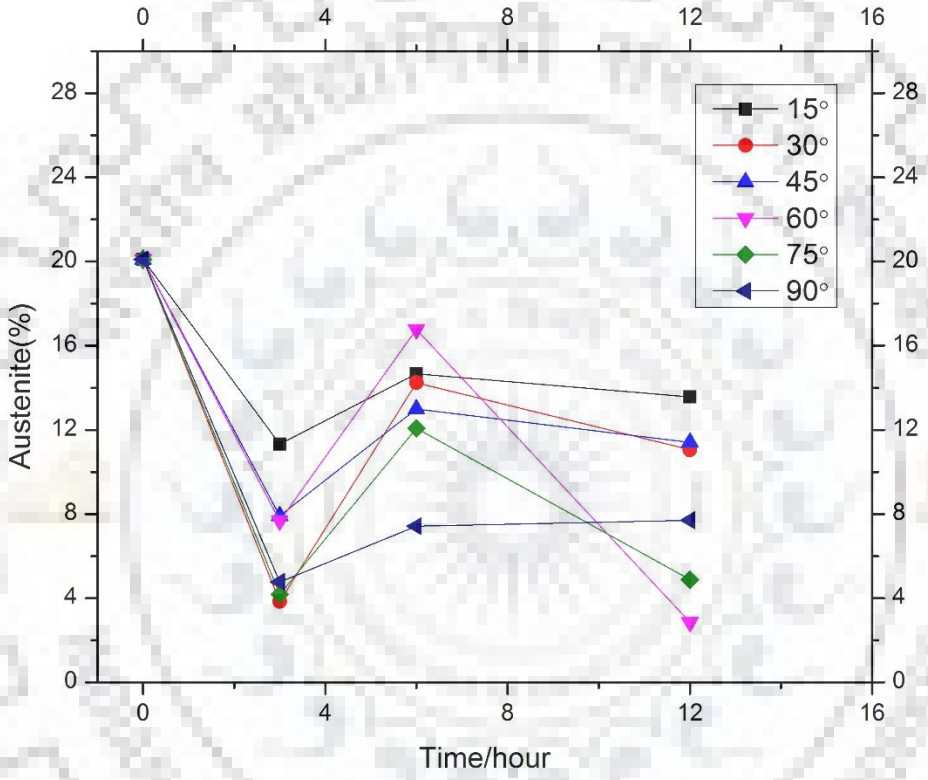

Fig 27: Fraction of austenite in the samples after erosion testing of 3hr, 6hr, 12hr

5.5.2 Williamson-Hall plots and modified Williamson-Hall plots

First four peaks of the austenite phase with hkl values (111), (002), (022) and (113) in the XRD spectra of as received sample and samples after erosion testing of 3hr, 6hr, and 12hr are taken into analysis. FWHM of those peaks calculated from Origin software. The Williamson-Hall plots for base sample and samples after 3hr, 6hr, and 12hr erosion testing are shown Figure 28.

(a)

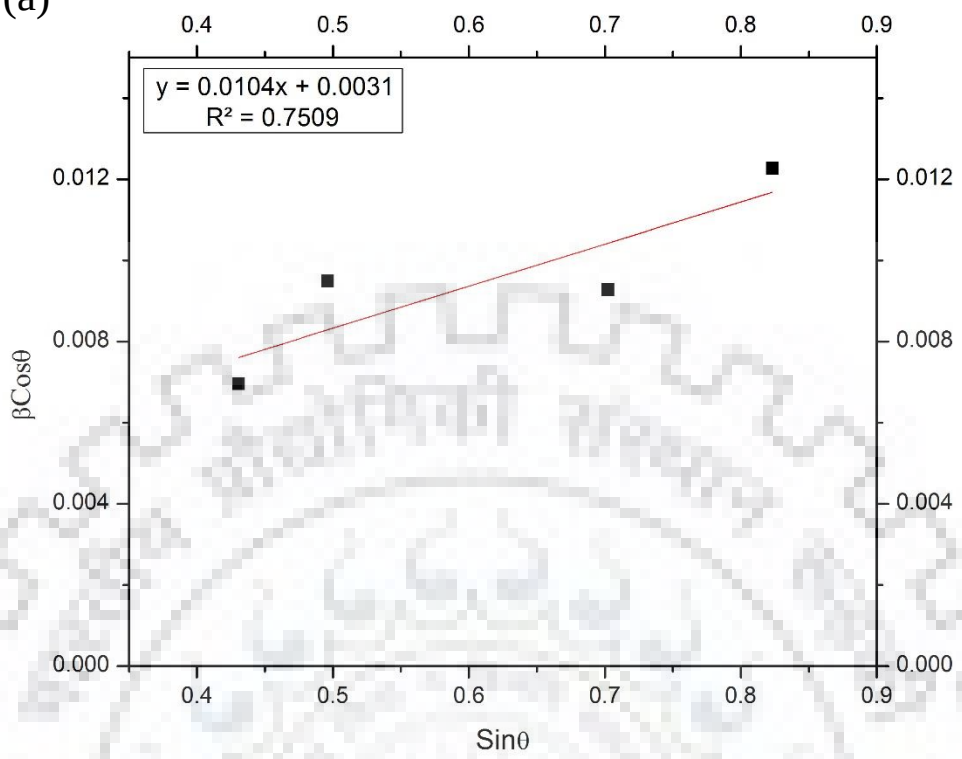
y = 0.0104x + 0.0031
R² = 0.7509
βCosθ
Sinθ
0.000
0.004
0.008
0.012
0.4
0.5
0.6
0.7
0.8
0.9

(b)

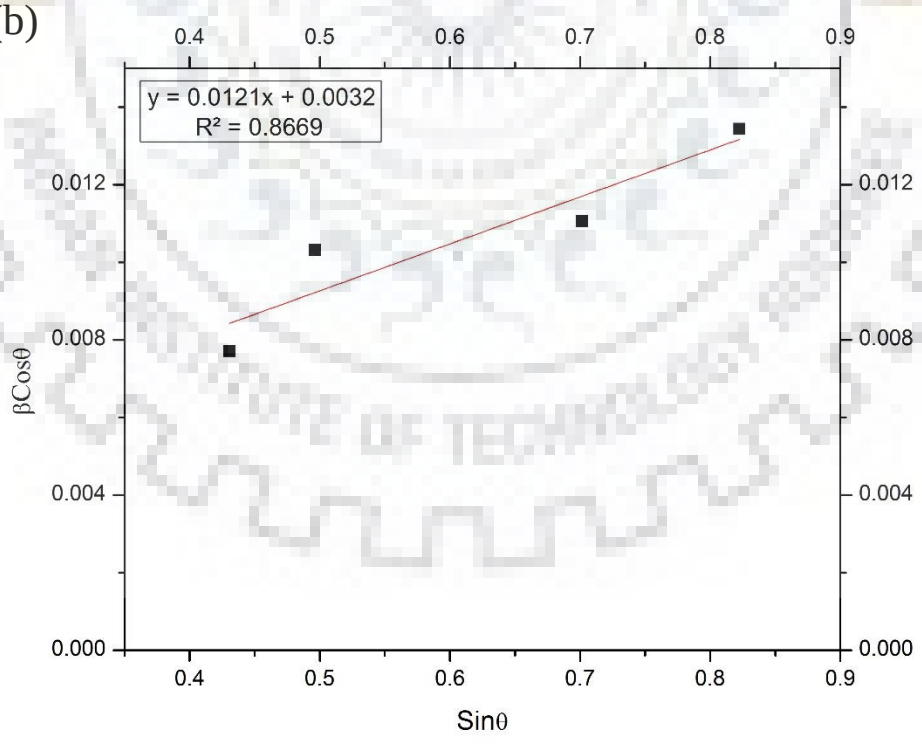
y = 0.0121x + 0.0032
R² = 0.8669
βCosθ
Sinθ
0.000
0.004
0.008
0.012
0.4
0.5
0.6
0.7
0.8
0.9

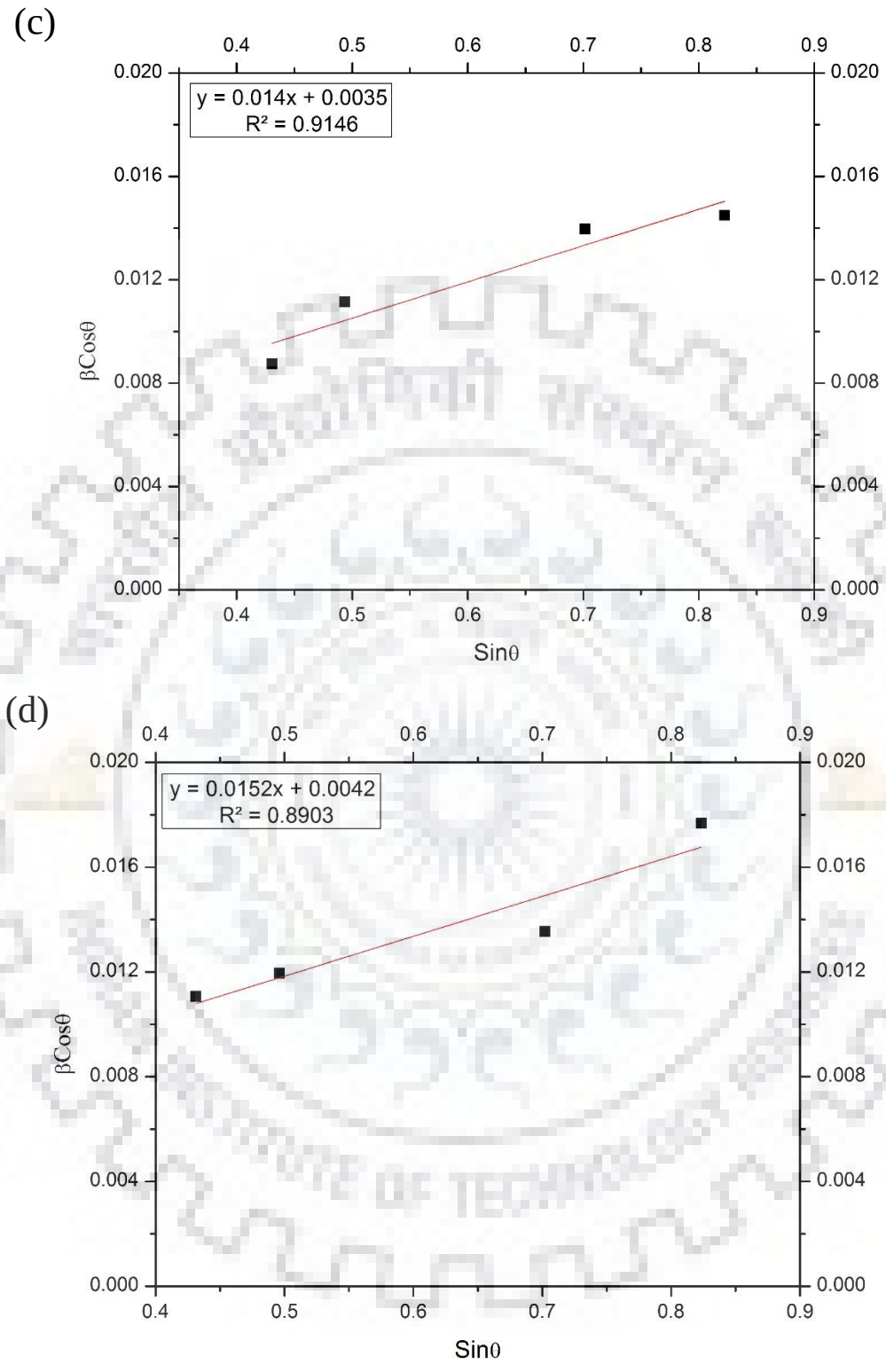

Fig 28: Williamson-Hall plots of as received sample (a) and samples after erosion testing of (b) 3hr, (c) 6hr & (d) 12hr

Crystallite size (D) and strain (ε) calculated from the Williamson- Hall plots and dislocation density calculated from Williamson and Smallman formula are tabulated in table 3.

Table 3: Crystallite size, strain and dislocation density of as received sample and sample after erosion testing of 3hr, 6hr, and 12hr

Sample description	Crystallite size (nm)	Strain	Dislocation density $\times 10^{17}$ (/m^2)
As received	51.9	0.0026	1.6
after 3 hr	50.3	0.0030	1.9
after 6 hr	46.0	0.0035	2.2
after 12 hr	38.3	0.0038	2.4

For calculation of modified Williamson-Hall plot again first four peaks were chosen. The elastic constant of single crystal austenite was taken as C_{11}= 204.6 GPa, C_{12} =137.7, and C_{44}=126.2[34] .

From ungar et. al.[32] values of contrast factor and q parameter for both screw and edge dislocation is obtained. The contrast factor for both edge dislocation and screw dislocation is given below:

For edge dislocation, C_{hkl}=0.2988 (1-1.72385H^2)

For screw dislocation, C_{hkl}=0.3104 (1-2.46093H^2)

Considering the austenite peaks with hkl values (111), (002), (022) and (113) H^2 value is calculated and then contrast factor is calculated for both edge dislocation and screw dislocation. Values of both the contrast factor are tabulated below in Table 4. Assuming equal amount of edge and screw dislocation, average contrast factor is calculated. Then values of ΔK is plotted against the values of K$\sqrt{C_{hkl}}$. These modified Williamson-Hall plot is shown in figure 29 (a), (b), (c), and (d).

Table 4: Contrast factor for both of edge and screw dislocation with respective hkl values

	hkl	$C_{hkl,Edge}$	$C_{hkl,Screw}$
1	111	0.126656	0.0558
2	002	0.2988	0.3104
3.	022	0.169692	0.11943
4.	113	0.217708	0.190315

(a)

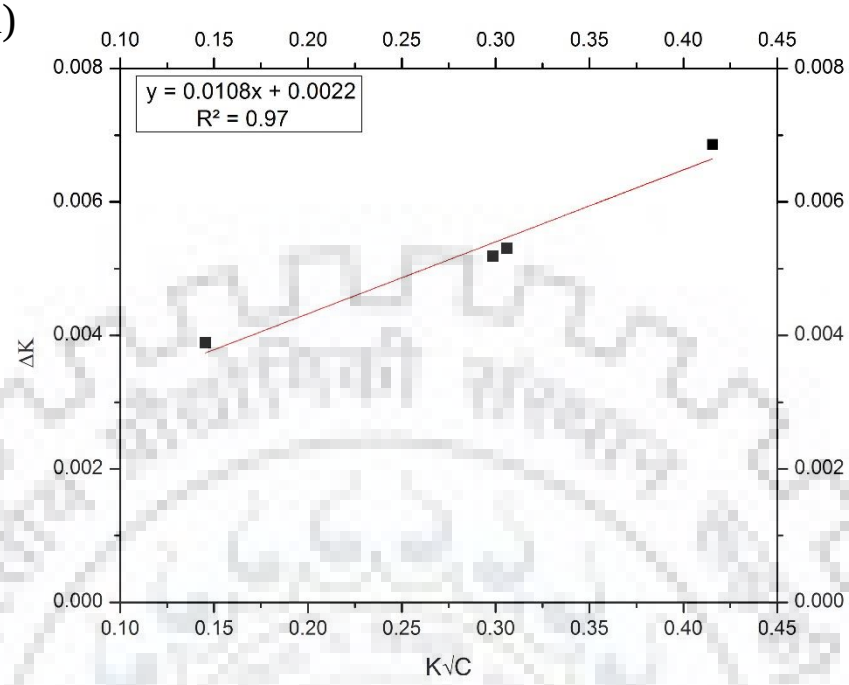
y = 0.0108x + 0.0022
R² = 0.97
ΔK
K√C
0.10
0.15
0.20
0.25
0.30
0.35
0.40
0.45
0.000
0.002
0.004
0.006
0.008

(b)

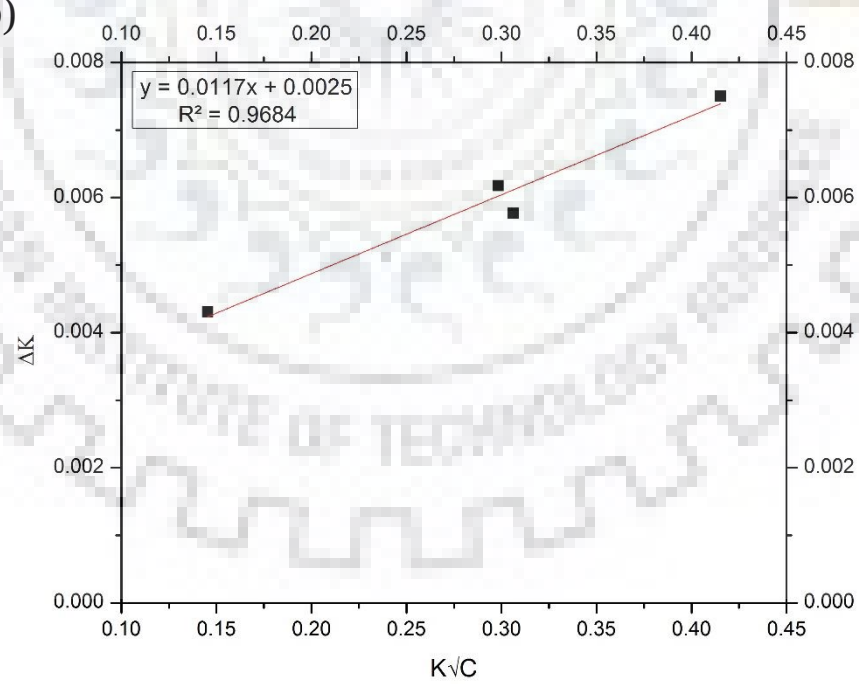
y = 0.0117x + 0.0025
R² = 0.9684
ΔK
K√C
0.10
0.15
0.20
0.25
0.30
0.35
0.40
0.45
0.000
0.002
0.004
0.006
0.008

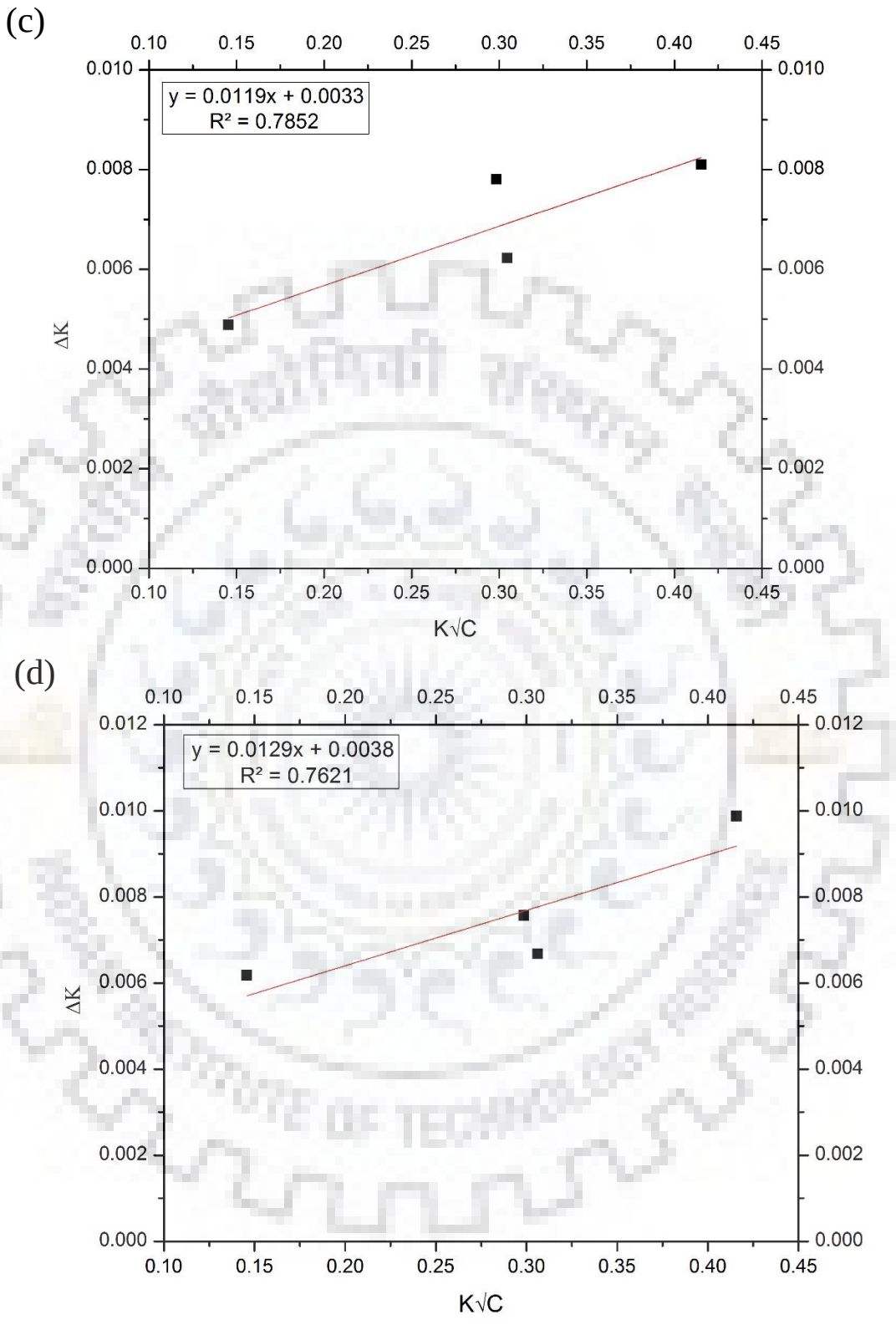

Fig 29: Modified Williamson-Hall plots of as receive sample and samples after erosion testing of 3hr, 6hr &12hr

Values of crystallite size is calculated from the intercept of the Williamson-Hall plot and modified Williamson-Hall plots as shown in Figures 28 and 29. These values are plotted against the erosion time as shown in figure 30. The trend in crystallite size is decreasing. A decrease in the crystallite size after erosion indicates plastic strain of the surface during erosion and it is in accordance with the strain calculated from the Williamson-Hall plot.

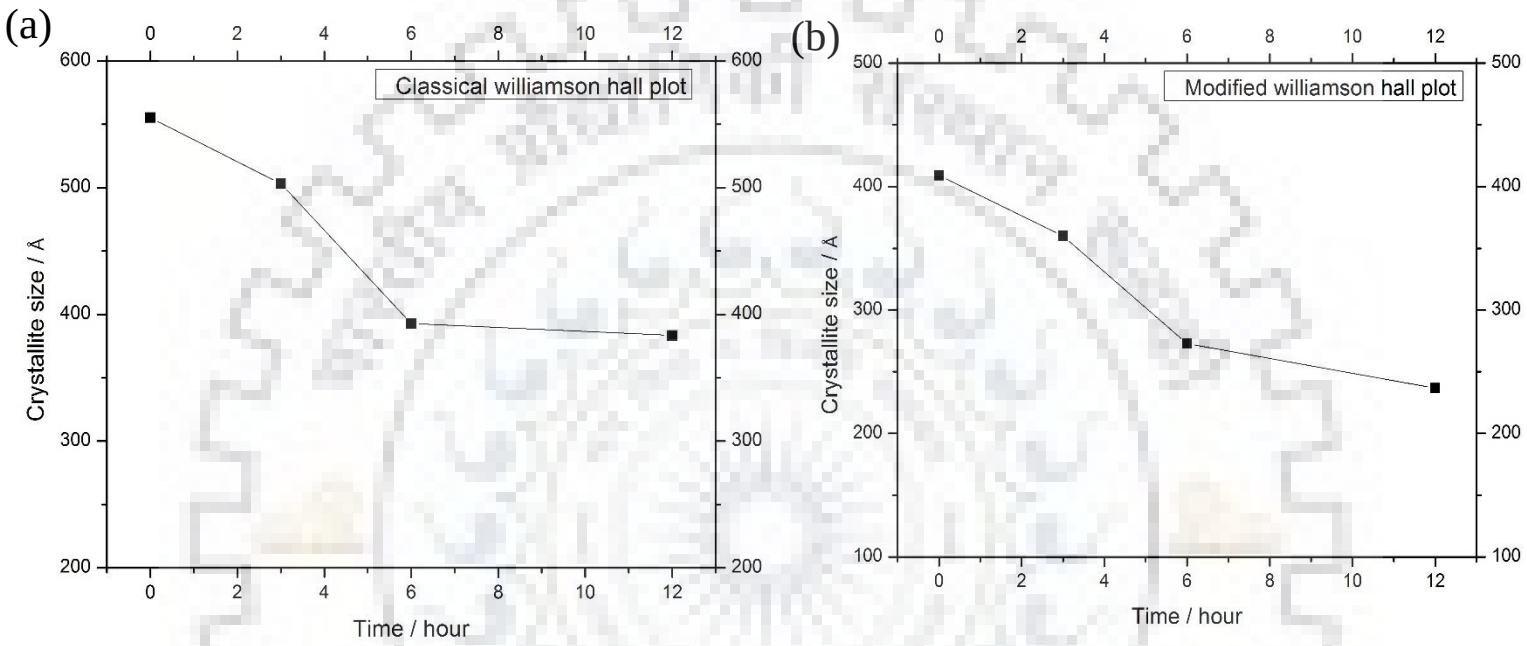

Fig 30: Variation of crystallite size with respect to erosion time calculated from (a) classical Williamson-Hall plot (b) calculated from modified Williamson-Hall plot

5.4.3 Determination of dislocation density

Dislocation density is calculated from both the Williamson and Smallman formula [26] and from modified Williamson-Hall equation. The more accurate results of dislocation density calculated from modified Williamson-Hall equation for base material and samples after 3hr, 6hr and 12hr erosion testing are plotted in Figure 31. Figure 31 shows that the dislocation density increases with erosion testing time. This result was expected as the high amount of subsurface deformation will lead increasing strain and dislocations with the erosion time.

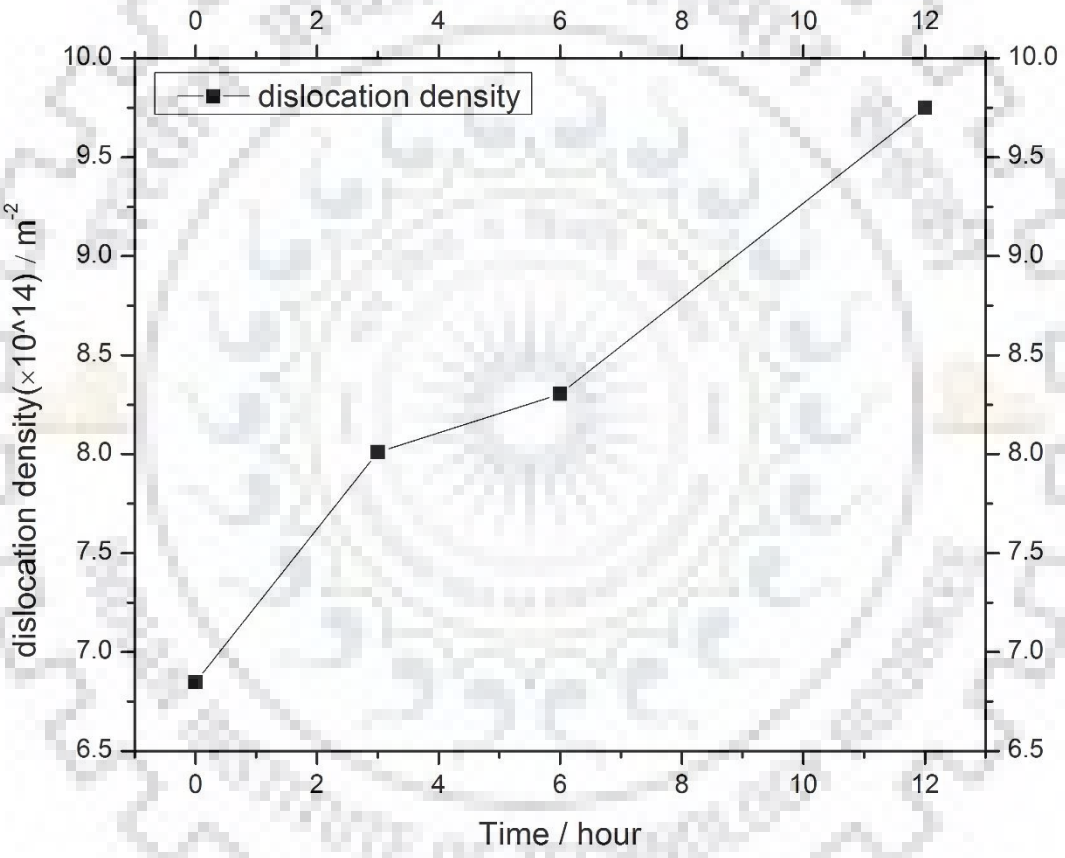

Fig 31: Variation of dislocation density with respect to erosion time calculated from the modified Williamson-Hall equation

CHAPTER 6

CONCLUSIONS

Investigations have been carried out to find the effect of slurry erosion on ultra-high strength bainitic steel. The studies have been conducted on as received samples for 6 different impact angles (15°, 30°, 45°, 60°, 75°, and 90°) and for 3 different time period (3hr, 6hr, and 12 hr).

The important conclusions drawn from the study are as follows:

1. Wear rate is observed to be affected by the impact angles in erosion test. A opposite trend is observed at high impact angles as compared to the low impact angles.
2. Cross-sections of the samples of 3hr, 6hr, and 12hr shows that average depth of erosion pits increases with the erosion time.
3. SEM images of the samples shows that micro-crack propagation in the direction of impact angle is the major wear mechanism of the ultra-high strength bainitic steel samples.
4. SEM images of sand used before and after the erosion test shows that sand particle significantly losses sharpness in the cutting edges.
5. Micro hardness test of the cross-sections of the samples shows significant increase in hardness near the surface for the sample after 12hr erosion testing
6. Quantitative phase analysis shows the fraction of the retained austenite is decreased initially and then marginal increasing- decreasing trend is observed due to the material removal of the surface.
7. Both Williamson-Hall plots and modified Williamson-Hall plot of the samples shows a decrease in crystallite size which is expected after the erosion test as strain is increasing with increasing duration of erosion test.
8. Dislocation density calculated from both Williamson-Hall plots and modified Williamson-Hall plot of the samples shows a increasing trend with time duration of erosion test. This hints the increasing amount of subsurface deformation during the erosion test.

SCOPE OF THE FUTURE WORK .

1. Samples consisting of tailored microstructures can be studied for their erosion performance.
2. The erodent particles used in this study were 297 μm size natural silica sand. The size can also be varied for further studies to understand the effect of particle size on erosion.
3. Comparative study of effect of various erodent particles like alumina etc. on erosion rate of ultra-high high strength bainitic steel can be carried out.
4. Effect of testing parameters eg. mass flow rate of erodent, speed of jet etc. on the erosion performance can also be studied.
5. Since the present study is restricted with only slurry erosion test, future work may be extended to sliding wear test, cavitation erosion and jet erosion

.

REFERENCES

1. N. P. Abbade, S. J. Crnkovic: "*Sand–water slurry erosion of API 5LX65 pipe steel as quenched from intercritical temperature*", Tribology international, 2000, vol. 33, p.p. 811–816.
2. N. Sekhar, M. K. Mohan., B. N. Reddy, and T. L. Reddy: "*Theoretical modeling of slurry erosive wear testing of HVOF thermally sprayed Inconel - titania coatings. Indian journal of science and technology*", 2012, vol. 5, p.p. 2872–2876.
3. H. McI Clark, R. J. Llewellyn: "*Assessment of the erosion resistance of steels used for slurry handling and transport in mineral processing applications*", Wear, 2001, vol. 250, p.p. 32–44.
4. M. C. Lina, L. S. Chang, H. C. Lin, C. H. Yang, K. M. Lin: "*A study of high-speed slurry erosion of NiCrBSi thermal-sprayed coating, Surface and coatings technology*", 2006, vol. 201, p.p. 3193–3198.
5. R. Dasgupta, B. K. Prasad, A. K. Jha, O. P. Modi, S Das, A. H. Yegneswaran: "*Effect of sand concentration on slurry erosion of steel*", Materials transactions JIM, 1998, vol. 39, p.p. 185–90.
6. S. Das, A. Haldar: "*Continuously cooled ultrafine bainitic steel with excellent strength-elongation combinations*", Metallurgical and materials transactions A, 2014, vol. 45, pp. 1844-1854.
7. B. Bhushan, "*Introduction to tribology*", Second edition, A john wiley & sons ltd., 2013, pp. 315-349.
8. E. F. Finkin: "*Abrasive wear, evaluation of wear testing*", ASTM STP 446, American Society for Testing and Materials", 1969, pp. 55-90.
9. A. Somi Reddy, B. N. Pramila Bai, K. S. S. Murthy, S. K. Biswas: "*Wear and seizure of binary Al-Si alloys*", 1994, Wear, vol 171,pp. 115-127
10. C. M. Hansson: "*Cavitation erosion, Lubrication, and Wear Technology*", ASM International, 1992, ASM Handbook Volume 18, pp. 1-4
11. A. Eghlimi, K. Raeissi, M. Shamanian: "*Tribocorrosion behavior of overlay welded super duplex stainless steel in chloride medium*", 2015, vol. 1, pp 1-18

12. A. S. Yadav, S. B. Mishra : "*Slurry erosive wear study of d-gun sprayed coatings on sae 431. International conference on control, computing, communication and materials",*ICCCCM , 2013

13. G. Singh, S. Kumar, S. K. Mohapatra: "*Erosion wear in a slurry pipe with multisized coal and bottom-ash slurries",* Materials today: Proceedings , 2017, Vol. 4, pp. 3565-3571.

14. S. Turenne, M. Fiset, J. Masounave: "*The effect of sand concentration on the erosion of materials by a slurry jet*",Wear , 1989, vol. 133, pp. 95–106

15. H. J. Amarendra, M. S. Prathap, S. Karthik, B. M. Darshan, Devaraj , P. C. Girish, V. T. Aruna: "*Combined slurry and cavitation erosion resistance of HVOF thermal spray coated stainless steel*", Materials Today: Proceedings, 2017, Vol. 4, pp. 465-470.

16. M. Lindgren , S. Siljander , R. Suihkonen , P. Pohjanne , J. Vuorinen : "*Erosion–corrosion resistance of various stainless steel grades in high-temperature sulfuric acid solution*", Wear, 2016, Vol. 364-365, pp. 10-21

17. B. Kishor, G. P. Chaudhari , S. K. Nath: "*Slurry erosion of thermo mechanically processed high speed slurry-pot erosion wear testing with large abrasive particles 13Cr4Ni stainless steel*", Tribology international, 2016, Vol. 93, pp. 50-57

18. N. Ojala , K. Valtonen , A. Antikainen , A. Kemppainen , J. Minkkinen , O. Oja , V. Kuokkala: "*Wear performance of quenched wear resistant steels in abrasive slurry erosion, Wear*", 2016, Vol. 354-355, pp. 21-31

19. A. A. Khan: "*Effect of slurry concentration on erosion wear of mild steel, International Journal In Applied Studies And Production Management*", 2015, Vol. 1, Issue 4

20. S. Dhawan, H. Singh, R. Singh: "*Erosion behaviour of stainless steel grade-316*", IOSR Journal of mechanical and civil engineering, 2015, pp. 58-63

21. N. Ojala, K. Valtonen, P. K. Reponen, P. Vuorinen, and V. Kuokkala: High speed slurry-pot erosion wear testing with large abrasive particles, Tribologia, 2015, Vol. 33, pp. 36-44.

22. N. Agarwal, G. P. Chaudhari , S. K. Nath : "*Slurry and cavitation erosion of HSLA steel processed by warm multidirectional forging and inter-critical annealing*", Tribology international, 2014, Vol. 70, pp. 18-25.

23. R. J. K. Wood, J. C. Walker, T. J. Harvey, S. Wang, S. S. Rajahram: "*Influence of microstructure on the erosion and erosion–corrosion characteristics of 316 stainless steel*", Wear, 2013, vol. 306, pp. 254–262.
24. E. Rabinowicz, "*Friction and wear of materials*", Wiley, N. York, 1965.
25. R. E. Winter, I. M. Hutchings, "*The erosion of ductile metals by spherical particles*", wear, 1974, vol. 8, pp. 181.
26. R. Bellman Jr., A. Levy: "*Erosion mechanism in ductile metals*",Wear, 1981, vol.70, pp. 1-70.
27. H. Sin, N. Saka, N. P. Suh: "*Abrasive wear mechanisms and the grit size effect*", Wear, 1979, vol. 55, pp. 163-190.
28. G. K Williamson, W. H Hall: "*X-ray line broadening from filed aluminium and wolfram*", Acta Metallurgica, 1953, vol. 1, pp. 22-31.
29. K. Venkateswarlu, M. Sandhyarani, T. A. Nellaipan, N. Rameshbabu: "*Estimation of crystallite size, lattice strain and dislocation density of nanocrystalline carbonate substituted hydroxyapetite by x-ray peak variance analysis*", Procedia Materials Science, vol. 5, 2014, pp. 212-221
30. G. Ribarik: "*Modeling of diffraction patterns based on microstructural properties*. PhD thesis, Department of materials physics, Eotvos lorand university, Hungary, 2008
31. T. Ungar: "*Dislocation densities, arrangements and character from X-ray diffraction experiments".* Materials Science & Engineering, A, 2001, vol. 309-310, pp. 14-22.
32. T. Ungar, I. Dragmoir, A. Revesz, and A. Borbely: "*The contrast factors of dislocations in cubic crystals: the dislocation model of strain anisotropy in practice"*, Journal of Applied Crystallography, 1999, vol. 32, pp. 992-1002.
33. E. Schafler, M. Zehetbauer, and T. Ungar: "*Measurement of screw and edge dislocation density by means of X-ray bragg profile analysis*". Materials science and engineering A, 2001, vol. 319-321, pp. 220-223.
34. Y. D. Wang, R. L. Peng and R. McGreevy: "*High anisotropy of orientation dependent residual stress in austenite of cold rolled stainless steel*", Scripta materialia, 1999, vol. 41, pp. 995-1000.